A Double-Moment Multiple-Phase Four-Class Bulk Ice Scheme. Part I: Description

Brad Schoenberg Ferrier

Universities Space Research Association, Mesoscale Dynamics and Precipitation Branch, Laboratory for Atmospheres, NASA Goddard Space Flight Center, Greenbelt, Maryland

(Manuscript received 12 November 1992, in final form 14 June 1993)

ABSTRACT

A detailed ice-phase bulk microphysical scheme has been developed for simulating the hydrometeor distributions of convective and stratiform precipitation in different large-scale environmental conditions. The proposed scheme involves 90 distinct microphysical processes, which predict the mixing ratios and the number concentrations of small ice crystals, snow, graupel, and frozen drops/hail, as well as the mixing ratios of liquid water on wet precipitation ice (snow, graupel, frozen drops). The number of adjustable coefficients has been significantly reduced in comparison with other bulk schemes. Additional improvements have been made to the parameterization in the following areas: 1) representing small ice crystals with nonzero terminal fall velocities and dispersive size distributions, 2) accurate and computationally efficient calculations of precipitation collection processes, 3) reformulating the collection equation to prevent unrealistically large accretion rates, 4) more realistic conversion by riming between different classes of precipitation ice, 5) preventing unrealistically large rates of raindrop freezing and freezing of liquid water on ice, 6) detailed treatment of various rime-splintering ice multiplication mechanisms, 7) a simple representation of the Hobbs–Rangno ice enhancement process, 8) aggregation of small ice crystals and snow, and 9) allowing explicit competition between cloud water condensation and ice deposition rates rather than using saturation adjustment techniques. For the purposes of conserving the higher moments of the particle distributions, preserving the spectral widths (or slopes) of the particle spectra is shown to be more important than strict conservation of particle number concentration when parameterizing changes in ice-particle number concentrations due to melting, vapor transfer processes (sublimation of dry ice, evaporation from wet ice), and conversion between different hydrometeor species.

The microphysical scheme is incorporated into a nonhydrostatic cloud model in Part II of this study. The model performed well in simulating the radar and microphysical structures of a midlatitude–continental squall line and a tropical–maritime squall system with minimal tuning of the parameterization, even though the vertical profiles of radar reflectivity differed substantially between these storms.

1. Introduction

The spatial distribution of diabatic heating by clouds has a direct impact upon the structure of tropical circulations, as well as those teleconnection patterns affecting midlatitude climate (Hartmann et al. 1984; DeMaria 1985; Lau and Peng 1987; Trenberth et al. 1988). In preparation for the Tropical Rainfall Measuring Mission (TRMM), cloud models are being used to develop algorithms for estimating distributions of diabatic heating in the tropics and subtropics from precipitation profiles retrieved using active (radar) and passive microwave observations from polar orbiting satellites (Simpson et al. 1988; Tao et al. 1990). However, airborne microwave measurements and radiative transfer calculations have shown that passive microwave signatures are highly sensitive to the microphysical structure of thunderstorms (Simpson et al. 1988; Yeh et al. 1990; Mugnai et al. 1990; Adler et al. 1991; Smith et al. 1992). If cloud models are to be used in these studies, they must represent with reasonable accuracy the hydrometeor structures of a wide variety of convective storms.

Recently, McCumber et al. (1991, hereafter referred to as M) made a thorough comparison of various two-class (Cotton et al. 1982; Chen 1983) and three-class (Lin et al. 1983, hereafter LFO; Rutledge and Hobbs 1984, hereafter RH) bulk ice schemes using the nonhydrostatic Goddard Cumulus Ensemble (GCE) model (Tao and Soong 1986; Tao and Simpson 1989). They found that the three-class ice parameterizations produced better agreement between simulated and observed structures of a fast-moving GATE squall system, such as the proportion of surface rainfall in the stratiform region and the intensity and structure of the radar bright band. They also noted, however, that different parameterizations must be used in order to simulate the hydrometeor structure of convective systems in different large-scale conditions. For example, the basic hydrometeor structure of tropical and subtropical maritime systems is better simulated using the parameterization of RH, whereas the hydrometeor structure

Corresponding author address: Dr. Brad S. Ferrier, Code 912, NASA Goddard Space Flight Center, Greenbelt, MD 20771.

of midlatitude continental storms is more accurately represented using the scheme of LFO (McCumber et al. 1991; Ferrier et al. 1991; Tao et al. 1991; Tao et al. 1993). Furthermore, reasonable agreement between simulated and observed radar reflectivity structures is often obtained only after "trial and error" adjustment of numerous coefficients in the parameterizations.

A new bulk microphysical scheme will be described that can simulate, with improved accuracy compared to other bulk treatments and with minimal adjustment of important coefficients, the diabatic heating and hydrometeor distributions of convective systems in widely varying large-scale environments. An equally important goal of this study is the formulation of a flexible bulk parameterization that can be modified in the future to incorporate findings from 1) observational studies using aircraft and radar data and 2) theoretical and numerical modeling studies using explicit spectral schemes. Substantive improvements in the parameterization of important microphysical processes will be presented. Because of the nature of bulk microphysical schemes, there are several possible ways of representing conversion processes between hydrometeor species. These approaches will be described and the best techniques will be documented. For example, in the formulation of those processes associated with conversion from one hydrometeor species to another, it will be shown that it is more important to preserve the basic spectral characteristics of the particle distributions than to maintain strict conservation of the particle number concentrations. This point is especially important if the modeler is interested in accurately simulating the higher-order moments of the particle distributions, such as those associated with precipitation rates (D^3-D^4; D is the particle diameter) and radar reflectivities (D^6).

2. Basic continuity equations

The microphysical parameterization calculates the mixing ratios of water vapor (q_v), cloud water in the form of small, nonprecipitating cloud droplets (q_w), raindrops (q_r), small ice crystals (q_i, also referred to as cloud ice), low-density ($\sim$0.1 g cm^{-3}) snow (q_s), moderate-density ($\sim$0.4 g cm^{-3}) graupel (q_g), and high-density ($\sim$0.9 g cm^{-3}) frozen drops/hail (q_h). To first order, the microphysical parameterization combines the main features that contrast the three-class ice schemes of RH (cloud ice, snow, and graupel) and LFO (cloud ice, snow, and hail). However, the model scheme also includes prognostic variables for the number concentrations of all ice hydrometeors (n_i for cloud ice, n_s for snow, n_g for graupel, and n_h for frozen drops), as well as the mixing ratios of liquid water on each of the precipitation ice species during wet growth and melting (q_{sw} for snow, q_{gw} for graupel, and q_{hw} for frozen drops). The inclusion of mixed-phase precipitation ice into the parameterization allows for more accurate radar calculations, and in the future it should be useful in passive radiometric calculations using linked cloud-radiation models (Mugnai et al. 1990; Adler et al. 1991; Smith et al. 1992).

Microphysical continuity equations for the mixing ratios of water vapor and all hydrometeor species, the number concentrations of all classes of ice, and the thermodynamic energy equation are summarized in appendix A. Table 1 contains a brief description of those processes that affect the mixing ratios of all hydrometeor species, while those processes that affect the number concentrations of the various ice categories are described in Table 2. Appendix E contains a complete list

TABLE 1. List of microphysical processes affecting hydrometeor mixing ratios.

Symbol	Source	Sink	Process
QCND	q_w q_v	q_v q_w	Condensation (QCND > 0) or evaporation (QCND < 0) of cloud water
QXEVP	q_v	q_x	Evaporation of rain and wet ice ($x = r, s, g, h$)
QINT	q_i	q_v	Nucleation of small ice
QXDEP	q_x q_v	q_v q_x	Deposition (QXDEP > 0) or sublimation (QXDEP < 0) of ice ($x = i, s, g, h$)
QIFM	q_i q_w	q_w q_i	Cloud water freezing (QIFM > 0) or melting of small ice (QIFM < 0)
QXFM	— q_{xw}	q_{xw} —	Freezing of liquid water on wet ice (QXFM > 0), melting of precipitation ice (QXFM < 0; $x = s, g, h$)
QXSHD	q_r	q_x	Raindrop shedding from wet ice ($x = s, g, h$)
QICNVS	q_s	q_i	Conversion of small ice to snow
QIHR	q_i	q_w	Hobbs–Rangno freezing of cloud water
QIHMX	q_i	q_x	Hallett–Mossop rime splintering of ice ($x = s, g, h$)
QRAUT	q_r	q_w	Cloud water autoconversion to rain
QXACW	q_x	q_w	Collection of cloud water ($x = r, i, s, g, h$)
QXACI	q_x	q_i	Collection of small ice ($x = r, s, g, h$)
QXACS	q_x	q_s	Collection of snow ($x = g, h$)
QIACR	q_h	q_r	Raindrop freezing by collection of small ice
QHACR	q_h	q_r	Collection of rain by frozen drops/hail
QXACRY	q_y	q_r	Raindrop freezing by collisions with q_x particles to form q_y particles ($x = s, g, h$; $y = s, g, h$)
QRACXY	q_y	q_x	Conversion from q_x particles to q_y particles by raindrop freezing ($x = s, g$; $y = g, h$)
QXACWY	q_y	q_w	Cloud water riming onto q_x particles to form q_y particles ($x = s, g$; $y = s, g, h$)
QWACXY	q_y	q_x	Conversion from q_x particles to q_y particles by cloud water riming ($x = s, g$; $y = g, h$)

TABLE 2. List of microphysical processes affecting hydrometeor number concentrations.

Symbol	Source	Sink	Process
NXEVP	—	n_x	Evaporation of wet ice ($x = s, g, h$)
NINT	n_i	—	Initiation of small ice
NXDEP	n_x	—	Deposition (NXDEP > 0), or
	—	n_x	sublimation (NXDEP < 0) of ice ($x = i, s, g, h$)
NIFM	n_i	—	Cloud water freezing (NIFM > 0), or
	—	n_i	melting of small ice (NIFM < 0)
NXSHD	—	n_x	Shedding of rain by complete melting of precipitation ice ($x = s, g, h$)
NICNV	—	n_i	Conversion of small ice to snow
NSCNV	n_s	—	
NIHR	n_i	—	Freezing of cloud water by ice enhancement (Hobbs–Rangno)
NIHMX	n_i	—	Hallett–Mossop rime splintering of ice ($x = s, g, h$)
NXACX	—	n_x	Aggregation of small ice and snow ($x = i, s$)
NXACI	—	n_i	Collection of small ice ($x = r, s, g, h$)
NSBR	n_s	—	Breakup of snow
NXACS	—	n_s	Collection of snow ($x = g, h$)
NIACR	n_h	—	Raindrop freezing by collection of small ice
NRACXY	—	n_x	Conversion from n_x particles to n_y
NXACRY	n_y	—	particles by raindrop freezing ($x = s, g; y = g, h$)
NWACXY	n_y	n_x	Conversion from n_x particles to n_y particles by cloud water riming ($x = s, g; y = s, g, h$)

of all of the symbols used in the equations throughout the paper that are not referenced in Tables 1 and 2. Hereafter, the characters X, Y, or Z in some of the microphysical process symbols, as well as the subscripts x, y, or z associated with other variables, denote multiple classes of hydrometeors. For example, the symbol QXDEP in Table 1 is a generic representation for the rates of deposition onto snow ($X = S$ for QSDEP, $x = s$ for q_s), graupel ($X = G$ for QGDEP, $x = g$ for q_g), and frozen drops ($X = H$ for QHDEP, $x = h$ for q_h). Note also that the mixing ratio of precipitation ice ($q_x = q_{xi} + q_{xw}$) predicted in the model is the sum of the mixing ratios of ice (q_{xi}) and liquid water (q_{xw}).

3. Particle characteristics

a. Size distributions

Following Williams and Wojtowicz (1982) and Ziegler (1985), the volume of cloud droplets (v) are assumed to have an exponential distribution of the form

$$n(v) = (n_w/v_0)\exp(-v/v_0), \qquad (3.1)$$

where v_0 $[=\rho q_w/(\rho_L n_w)]$ is the mean droplet volume, n_w is the droplet number concentration, and ρ_L is the density of liquid water. In many other bulk schemes cloud droplets are assumed to be monodisperse.

The size distributions for rain and all of the ice species are represented by gamma functions, where

$$n_x(D) = n_{ox}D_x^{\alpha_x}\exp(-\lambda_x D_x); \qquad (3.2)$$

n_{0x} is the intercept, λ_x is the slope, and α_x is the shape parameter of the distribution.[1] The shape parameters of the particle distributions are independently specified for each of the hydrometeor categories, but remain constant throughout a given model simulation. Most of the model simulations have assumed exponential ($\alpha_x = 0$) distributions for each of the different ice hydrometeors, whereas the raindrop size spectra are typically represented by either exponential (Marshall and Palmer 1948) or gamma (Willis 1984) distributions. Future development of this scheme will include the number concentrations of raindrops as an additional prognostic variable, where explicit schemes (e.g., Kogan 1991) will be used as a means of improving such bulk approaches as Ziegler (1985). Based upon the modeling of cirrus clouds by Starr and Cox (1985), the functional relationship of (3.2) is also assumed for the particle distributions of small ice crystals, rather than assuming a monodisperse distribution for cloud ice as in other bulk schemes.

Since mixing ratios (q_x) and number concentrations (n_x) are calculated for each ice category, the slope and intercept of a given particle distribution are, respectively,

$$\lambda_x = \left[\frac{\Gamma(1+\alpha_x+d_x)c_x n_x}{\Gamma(1+\alpha_x)\rho q_x}\right]^{1/d_x}, \qquad (3.3)$$

$$n_{ox} = \frac{n_x\lambda_x^{1+\alpha_x}}{\Gamma(1+\alpha_x)}, \qquad (3.4)$$

where $m_x(D_x) = c_x D_x^{d_x}$ is the assumed mass–diameter relationship of the dry ice particles, and Γ is the gamma function. Precipitation ice is typically assumed to be spherical with $c_x = \pi/6\cdot\rho_x$ and $d_x = 3$ for $x = s, g,$ and h (snow, graupel, and hail/frozen drops). For cloud ice, $c_i = 0.044$ and $d_i = 3$ for bullet rosettes (Heymsfield 1972; Starr and Cox 1985), which is believed to be the dominant small ice habit in thunderstorm anvils (Heymsfield and Knollenberg 1972). Although different parameterized rain distributions have been tested, the gamma distributions of Willis (1984) are assumed with $\alpha_r = 2.5$, where (in cgs units)

$$\lambda_r = 3.483(\rho q_r)^{-0.168}, \qquad (3.5)$$

$$n_{or} = 30.07(\rho q_r)^{-0.092}. \qquad (3.6)$$

b. Terminal fall speeds

The general relationship used to represent the terminal fall velocities of cloud ice, rain, and precipitation ice (snow, graupel, and hail/frozen drops) is

[1] Note that the shape parameter is defined as $\alpha_x - 1$ in other mathematical representations of the gamma function (e.g., Verlinde et al. 1990).

$$V_x(D_x) = \gamma a_x D^{b_x} \exp(-f_x D_x), \tag{3.7}$$

$\gamma = (\rho_0/\rho)^{1/2}$, ρ is the air density, and ρ_0 is the surface air density. Table 3 lists the values of the coefficients a_x and f_x and exponent b_x assumed for each hydrometeor species, the range of mass-weighted terminal fall velocities (defined later in this subsection), and the reference for each velocity–diameter (V–D) relationship.

As Potter (1991) recently showed, different fall speed relationships may be derived based upon different assumptions regarding the appropriate diameter of the ice particle. For example, Locatelli and Hobbs (1974) cite V–D and velocity–mass (V–m) fall speed relationships for different types of snow and graupel. The particle diameters in their study refer to the maximum particle dimension, which can differ markedly from the mean spherical diameter assumed in the bulk schemes. The snow fall speed coefficients are derived by substituting the assumed mass–diameter relationship for snow in the current scheme of

$$m_s = \pi/6\rho_s D_s^3 \tag{3.8}$$

with $\rho_s = 0.1$ g cm^{-3} into

$$V_s(D_s) = 195.8 m_s^{0.14} \quad \text{(cgs units)}, \tag{3.9}$$

which is the corrected V–m fall speed relationship (see Potter 1991) for "graupel-like snow of hexagonal type" from Locatelli and Hobbs (1974). This technique is a variation of Potter's approach, where he used the density of liquid water instead of snow in (3.8) for the purpose of estimating particle fall velocities as functions of their melted diameter. The fall speed relationship for ice crystals was obtained by matching the fall speed of a 200-μm snow particle with an assumed fall speed of 10 cm s^{-1} for a 50-μm ice crystal, resulting in similar mass-weighted fall speeds between cloud ice and snow.

Weighted fall velocities are used to calculate the vertical flux convergence terms for falling hydrometeors. For example, the change in the mixing ratio of a hydrometeor species is

$$\frac{\partial q_x}{\partial t} = -\frac{1}{\rho}\nabla\cdot(\rho \mathbf{V} q_x) + \mathrm{TURB}(q_x) + \frac{1}{\rho}\frac{\partial(\rho q_x [V]_q)}{\partial z} + \frac{dq_x}{dt}, \tag{3.10}$$

where the terms on the right side of (3.10) represent the changes in q_x by advection, turbulent diffusion, vertical flux convergence, and microphysical sources and sinks, respectively. Equation (3.10) is used to advect dependent variables q_x and q_{xw}, and q_{xi} is calculated from $q_x - q_{xw}$. In calculating the vertical flux convergence of q_x,

$$[V]_q = \gamma a_x \frac{\Gamma(1+\alpha_x+d_x+b_x)}{\Gamma(1+\alpha_x+d_x)} \frac{\lambda_x^{(1+\alpha_x+d_x)}}{(\lambda_x+f_x)^{(1+\alpha_x+d_x+b_x)}} \tag{3.11}$$

is the mass-weighted terminal velocity of the hydrometeors (Srivastava 1967) using (3.2) and (3.7). A similar prognostic equation is used for the advection of number concentration,

$$\frac{\partial n_x}{\partial t} = -\nabla\cdot(\mathbf{V} n_x) + \mathrm{TURB}(n_x) + \frac{\partial(n_x[V]_n)}{\partial z} + \frac{dn_x}{dt}, \tag{3.12}$$

except that

$$[V]_n = \gamma a_x \frac{\Gamma(1+\alpha_x+b_x)}{\Gamma(1+\alpha_x)} \frac{\lambda_x^{(1+\alpha_x)}}{(\lambda_x+f_x)^{(1+\alpha_x+b_x)}} \tag{3.13}$$

is the terminal velocity of the hydrometeors weighted by number concentration (Srivastava 1978).

c. *Densities of wet ice*

Although a constant density for dry snow, graupel, and frozen drops is assumed, the density of wet precipitation ice can change as a result of a variable mixture of liquid water and ice. Two different assumptions are made in deriving the densities of wet ice.

For porous snow and graupel, liquid water is assumed to be uniformly soaked throughout the volume of an ice particle, which implies that the volumes are the same between wet (water and ice) and dry (ice only) particles of equal ice mass. The total volume of spherical precipitation particles having a size distribution given by (3.2) is

$$\mathrm{VOL}_x = \int_0^\infty \pi/6 D_x^3 n_{ox} D_x^{\alpha_x} e^{-\lambda_x D_x} dD_x = \pi/6 \frac{\Gamma(4+\alpha_x)}{\Gamma(1+\alpha_x)} n_x \lambda_x^{-3}. \tag{3.14}$$

TABLE 3. Terminal fall velocity relationships. Range of mass-weighted fall speeds $[V_x]_q$ are calculated at the surface (i.e., $\gamma = 1$).

Hydrometeor	Coefficients in (3.7) a_x	b_x	f_x	$[V_x]_q$ (cm s^{-1})	Reference(s)
Rain	4854	1	1.95	170–730	Uplinger (1981)
Cloud ice	336	.6635	0	13–61	See text
Snow	129.6	.42	0	32.5–85.5	See text
Graupel	351.2	.37	0	104–314	Locatelli & Hobbs (1974)
Frozen drops/hail	1094.3	.6384	0	136–922	Böhm (1989), Matson & Huggins (1980)

In the following discussion, variables with the subscripts x and xi represent those quantities associated with the water–ice mixture and dry ice, respectively. Since the number concentrations and particle volumes are the same between the wet and dry distributions (i.e., $n_x = n_{xi}$ and $\mathrm{VOL}_x = \mathrm{VOL}_{xi}$, respectively), it follows from (3.14) that the slopes of the wet and dry particle distributions are the same ($\lambda_x = \lambda_{xi}$). Using (3.3) to represent λ_x and λ_{xi} and noting that $q_x = q_{xi} + q_{xw}$, then the bulk density of wet snow and wet graupel is

$$\rho_x = \rho_{xi}/(1 - F_{xw}), \tag{3.15}$$

where F_{xw} is the liquid water fraction of the snow and graupel (see A.12), $\rho_{si} = 0.1$ g cm^{-3} ($x = s$), and $\rho_{gi} = 0.4$ g cm^{-3} ($x = g$).

In contrast, liquid water is assumed to be uniformly coated around high density frozen drops/hail because there is very little air within the interior of these (dry) particles. The liquid water content is therefore proportional to the difference in volumes between the wet (water and ice) frozen drops and their ice cores, such that

$$\rho q_{hw} = (\mathrm{VOL}_h - \mathrm{VOL}_{hi}). \tag{3.16}$$

The bulk density of wet frozen drops/hail is obtained by using (3.3) and (3.14) to represent VOL_h and VOL_{hi} ($\rho_{hi} = 0.9$ g cm^{-3}):

$$\rho_h = \frac{\rho_{hi}}{1 - (1 - \rho_{hi}/\rho_L)F_{hw}}. \tag{3.17}$$

Note that the density and the liquid water fraction of wet precipitation ice are calculated from the mixing ratios of the total water–ice (q_x) and liquid water constituents (q_{xw}).

4. Improved microphysical processes

Improvements made to the most important microphysical processes are discussed in this section. Appendix B contains additional discussion and extended derivations of some of these processes, as well as descriptions of the other microphysical processes listed in Tables 1 and 2.

a. Collection of precipitation

The discussion in this subsection is separated into three parts. First, a new method for calculating the collection rates associated with collisions between different classes of precipitation is described that is accurate and computationally efficient. Second, this technique is applied to more complicated three-component freezing processes involving collisions between ice particles and supercooled raindrops. Finally, a modified collection kernel is proposed in situations where hydrometeors are removed rapidly by large accretion rates.

1) BINARY (TWO COMPONENT) ACCRETION PROCESSES (QXACZ, NXACZ)

The change in the mixing ratio of species X due to collection of species Z is

$$\mathrm{QXACZ} = \rho^{-1} \iint \frac{\pi}{4} E_{xz}(D_x + D_z)^2 \times |V_x - V_z| c_z D_z^{d_z} n_z(D_z) n_x(D_x) dD_z dD_x, \tag{4.1}$$

where QXACZ is used to represent the microphysical processes of QSACR, QGACR, QHACR, QGACS, and QHACS. Because this collection kernel has no straightforward analytic solution, simple approximations have been used in previous models to evaluate this integral (Wisner et al. 1972; Flatau et al. 1989; Murakami 1990). Verlinde et al. (1990) performed a detailed mathematical analysis of this collection kernel[2] and described the errors associated with various approximations.

The approach in this parameterization is to solve these equations numerically and store the solutions in lookup tables. Substituting for $n_x(D_x)$ and $n_z(D_z)$ using (3.2), as well as for $V_x(D_x)$ and $V_z(D_z)$ using (3.7), the collection kernel in (4.1) is

$$\mathrm{QXACZ} = \frac{\pi}{4\rho} \gamma c_z n_{ox} n_{oz} \cdot \Lambda_q(\lambda_x, \lambda_z) \cdot \Delta V_q(\lambda_x, \lambda_z), \tag{4.2}$$

where

$$\Lambda_q = \Lambda_q(\lambda_x, \lambda_z) = \frac{\Gamma(1 + \alpha_x)\Gamma(6 + \alpha_z)}{\lambda_x^{1+\alpha_x} \lambda_z^{6+\alpha_z}} + 2\frac{\Gamma(2 + \alpha_x)\Gamma(5 + \alpha_z)}{\lambda_x^{2+\alpha_x} \lambda_z^{5+\alpha_z}} + \frac{\Gamma(3 + \alpha_x)\Gamma(4 + \alpha_z)}{\lambda_x^{3+\alpha_x} \lambda_z^{4+\alpha_z}}, \tag{4.3}$$

[2] A constant collection efficiency independent of particle diameter was assumed in their study.

TABLE 4. Range of λ_x in accretion tables.

Hydrometeor	α_x	$(\lambda_x)_1$	$(\lambda_x)_{20}$
Rain	0	10	100
	2.5	20	150
Snow	0	10	100
Graupel	0	5	100
Frozen drops	0	5	100

$$\Delta V_q = \Delta V_q(\lambda_x, \lambda_z) = \Lambda_q^{-1} \iint E_{xz}(D_x + D_z)^2 |a_x D_x^{b_x} e^{-f_x} - a_z D_z^{b_z} e^{-f_z}| D_z^{\alpha_z + d_z} e^{-\lambda_z D_z} dD_z D_x^{\alpha_x} e^{-\lambda_x D_x} dD_x \quad (4.4)$$

is a scaled velocity associated with the difference in the terminal fall speeds of the colliding hydrometeor species, and $c_z = \pi/6\rho_z$ and $d_z = 3$ are assumed for precipitation. The term Λ_q is equal to the numerator in (4.4) but without the factor associated with the absolute value of the particle fall speed differences. The advantage of (4.2) over (4.1) is that the scaled velocity ΔV_q is a function only of the slopes of the collector (λ_x) and collected (λ_z) particle distributions, and ΔV_q varies much more gradually over a wide range of λ_x and λ_z than QXACZ. For each collection process, a two-dimensional lookup table is created that contains numerical solutions of ΔV_q at 20 different logarithmically spaced values of λ_x and λ_z, where

$$(\lambda_x)_j = \chi^{j-1}(\lambda_x)_1 \quad (4.5)$$

and

$$\chi = \exp\{[\ln(\lambda_x)_1 - \ln(\lambda_x)_{20}]/19\}. \quad (4.6)$$

Table 4 contains a list of the values of $(\lambda_x)_1$ and $(\lambda_x)_{20}$ for rain ($\alpha_r = 0$ and $\alpha_r = 2.5$ distributions), snow, graupel, and frozen drops/hail. Accurate estimates of ΔV_q are obtained by bilinear interpolation with respect to the tabulated values of λ_x and λ_z. Solutions for ΔV_q are calculated by numerically integrating (4.1) over 50 discrete size intervals in D_x and D_z with $D_x \leqslant 20/\lambda_x$ and $D_z \leqslant 20/\lambda_z$. Tests indicate that the maximum relative error in calculating QXACY using this approach is less than 5%, which is far more accurate than those approximations typically used in other bulk schemes, as discussed in Verlinde et al. (1990). The use of lookup tables also makes this technique computationally efficient. In addition, these tables only need to be created once and can be used in many model simulations, so long as the particle fall speeds and the range of λ's (Tables 3 and 4) are unchanged. The lookup tables will be expanded in the future to include a larger range of λ.

In conditions where graupel and frozen drops are growing by cloud water riming above the freezing level, it is possible that the larger collector particles are wet (wet growth), while the smaller collector particles remain dry (dry growth). Since the collection efficiency of snow (E_{xs}) depends upon whether the surface of the collector particles is wet or dry, a modification to the collection kernel in (4.2) is described in appendix B for calculating the collection of snow by graupel (QGACS) and frozen drops (QHACS) in the presence of supercooled cloud water.

2) Three-component accretion processes—The freezing of raindrops (QXACRY, QRACXY, NRACXY, QIACR, NIACR)

In the parameterizations of LFO and RH, collisional freezing of raindrops was the source of either snow or rimed ice (i.e., graupel in RH, hail in LFO) based upon somewhat arbitrary threshold mixing ratios of rainwater and snow. The experiences of the Goddard cloud modeling group, however, indicate that the use of different threshold mixing ratios can have an important impact upon the microphysical structure of the simulated storms. Precipitation produced by collisional freezing of rain should be classified according to the densities of the resultant ice particles. For example, collisions between populations of rain and snow should simultaneously produce snow (large snowflakes collecting smaller drops), graupel (snow colliding with similar-sized drops), and frozen drops (large drops collecting smaller snow), whereas collisions between graupel and rain populations should produce either graupel (graupel collecting smaller drops) or frozen drops (large drops collecting graupel).

Such a process is considered in the current parameterization by assuming that the liquid water from the raindrop is evenly distributed throughout the volume of the collided ice particle before freezing. Equating the particle masses of an ice particle of diameter D_x colliding with a raindrop of diameter D_r, then

$$\pi/6(\rho_x D_x^3 + D_r^3) = \pi/6\rho_y Dx^3, \quad (4.7)$$

where ρ_y is the density of the newly formed ice-drop mixture ($\rho_L = 1$ for drops), which is classified as either snow $[\rho_y \leqslant 0.5(\rho_s + \rho_g)]$, graupel $[0.5(\rho_s + \rho_g) < \rho_y < 0.5(\rho_g + \rho_h)]$, or frozen drops $[\rho_y \geqslant 0.5(\rho_g + \rho_h)]$. Substituting these values of ρ_y into (4.7) gives a range of drop sizes ($D_1 \leqslant D_r \leqslant D_2$) as a function of the size of the colliding ice particle (D_x). Table 5 lists the values of D_1 and D_2 for each of the accretion processes. The production of ice (species Y) by the freezing of raindrops colliding with other ice particles (species X, which can be the same ice class as Y) then becomes

$$\text{QXACRY} = \frac{\pi^2}{24\rho} \gamma n_{ox} n_{or} \cdot \Lambda_q(\lambda_x, \lambda_r) \cdot \Delta V_q(\lambda_x, \lambda_r), \quad (4.8)$$

$$\Delta V_q(\lambda_x, \lambda_r) = \Lambda_q^{-1} \int_0^\infty D_x^{\alpha_x} e^{-\lambda_x D_x} dD_x \times \int_{D_1}^{D_2} E_{xr}(D_x + D_r)^2 |a_x D_x^{b_x} - a_r D_r^{b_r} e^{-f_r}| D_r^{3+\alpha_r} e^{-\lambda_r D_r} dD_r, \quad (4.9)$$

TABLE 5. Values of D_1 and D_2 in (4.8)–(4.13).

D_1	D_2	Process(es)
0	$[0.5\,(\rho_{gi} - \rho_{si})]^{1/3}D_s$	QSACRS
$[0.5\,(\rho_{gi} - \rho_{si})]^{1/3}D_s$	$[0.5\,(\rho_{gi} + \rho_{hi}) - \rho_{si}]^{1/3}D_s$	QSACRG
$[0.5\,(\rho_{g} + \rho_{hi}) - \rho_{si}]^{1/3}D_s$	∞	QSACRH
0	$[0.5\,(\rho_{hi} - \rho_{gi})]^{1/3}D_g$	QGACRG
$[0.5\,(\rho_{hi} - \rho_{gi})]^{1/3}D_g$	∞	QGACRH
$[0.5\,(\rho_{gi} - \rho_{si})]^{1/3}D_s$	$[0.5\,(\rho_{gi} + \rho_{hi}) - \rho_{si}]^{1/3}D_s$	QRACSG, NRACSG
$[0.5\,(\rho_{gi} + \rho_{hi}) - \rho_{si}]^{1/3}D_s$	∞	QRACSH, NRACSH
$[0.5\,(\rho_{hi} - \rho_{gi})]^{1/3}D_g$	∞	QRACGH, NRACGH

in which $\Lambda_q(\lambda_x, \lambda_r)$ is given by (4.3). Conversion of mixing ratio and number concentration, respectively, from one category of ice (species X) to another (species Y) as a result of collisional freezing of rain is

$$\mathrm{QRACXY} = \frac{\pi}{4\rho}\gamma c_x n_{ox} n_{or}\cdot\Lambda_q(\lambda_r, \lambda_x)\cdot\Delta V_q(\lambda_r, \lambda_x), \tag{4.10}$$

$$\Delta V_q(\lambda_r, \lambda_x) = \Lambda_q^{-1}\int_0^\infty D_x^{\alpha_x+d_x}e^{-\lambda_x D_x}dD_x \times\int_{D_1}^{D_2}E_{xr}(D_x+D_r)^2|a_x D_x^{b_x} - a_r D_r^{b_r}e^{-f_r}|D_r^{\alpha_r}e^{-\lambda_r D_r}dD_r, \tag{4.11}$$

$$\mathrm{NRACXY} = \mathrm{NXACRY} = \frac{\pi}{4}\gamma n_{ox} n_{or}\cdot\Lambda_n(\lambda_r, \lambda_x)\cdot\Delta V_n(\lambda_r, \lambda_x), \tag{4.12}$$

$$\Delta V_n(\lambda_r, \lambda_x) = \Lambda_n^{-1}\int_0^\infty D_x^{\alpha_x}e^{-\lambda_x D_x}dD_x \times\int_{D_1}^{D_2}E_{xr}(D_x+D_r)^2|a_x D_x^{b_x} - a_r D_r^{b_r}e^{-f_r}|D_r^{\alpha_r}e^{-\lambda_r D_r}dD_r, \tag{4.13}$$

where $\Lambda_q(\lambda_r, \lambda_x)$ in (4.11) and $\Lambda_n(\lambda_r, \lambda_x)$ in (4.13) are given by expressions analogous to (4.3) and (B.4), respectively. Values of ΔV_q and ΔV_n in (4.9), (4.11), and (4.13) are also represented by two-dimensional lookup tables at the same discrete values of λ_r and λ_x as in Table 4. The tabulated values of ΔV_q also conserve hydrometeor mass, such that the following microphysical relationships,

$$\mathrm{QSACR} = \mathrm{QSACRS} + \mathrm{QSACRG} + \mathrm{QSACRH} \tag{4.14}$$

and

$$\mathrm{QGACR} = \mathrm{QGACRG} + \mathrm{QGACRH}, \tag{4.15}$$

are accurate to a precision of three orders of magnitude.

Another three-component freezing process is the production of frozen raindrops due to collisions with small ice crystals (QIACR, NIACR). As in other schemes (e.g., LFO; RH; Cotton et al. 1986, hereafter referred to as COT), the effects of ice crystal fall speeds upon the collection kernel are neglected because raindrop fall speeds are much faster. The errors associated with this assumption are small, given the limited size of the ice crystals. Ice crystals are converted into snow when $\lambda_i < 50\ \mathrm{cm}^{-1}$ (see section 4f). Future refinements of the scheme will include lookup tables for the collection of ice crystals. It is assumed, however, that raindrops effectively collect only those ice crystals larger than a critical size (D_{ri}, where $E_{ri} = 0$ for $D_r < D_{ri}$ and $E_{ri} = 1$ for $D_r \geqslant D_{ri}$), such that

$$\mathrm{QIACR} = \frac{\pi^2}{24\rho}\gamma a_r n_{or} n_i \Gamma(6+\alpha_r+b_r)(\lambda_r + f_r^{-(6+\alpha_r+b_r)}) \times\{1-\gamma^*[6+\alpha_r+b_r, (\lambda_r+f_r)D_{ri}]\}, \tag{4.16}$$

$$\mathrm{NIACR} = \frac{\pi}{4\rho}\gamma a_r n_{or} n_i \Gamma(3+\alpha_r+b_r)\lambda_r^{-(3+\alpha_r+b_r)} \times\{1-\gamma^*[3+\alpha_r+b_r, (\lambda_r+f_r^{-(3+\alpha_r+b_r)})D_{ri}]\}, \tag{4.17}$$

where $\gamma^*(x, y)$ is the incomplete gamma function[3] and D_{ri} is 40 μm (Lew et al. 1985). This assumption is important because many of the ice crystals that coexist with raindrops are small ($D_i < D_{ri}$), resulting in effective collection efficiencies (E_{ri}) much smaller than unity.

3) MODIFIED COLLECTION KERNEL FOR RAPID ACCRETION RATES

Although the techniques used to calculate instantaneous accretion rates are much more accurate than in previous parameterizations, unrealistically large changes in hydrometeor mixing ratio (Δq_z) occasionally occur when multiplying the accretion rates (QXACZ) by the model time step[4] Δt, such that the relative change in the hydrometeor mixing ratio,

[3] $\gamma^*(x, y) \equiv \gamma(x, y)/\Gamma(x)$, where $\gamma(x, y) = \int_0^y t^{x-1}e^{-t}dt$.

[4] Time steps typically used in the GCE model range from 5 to 10 s.

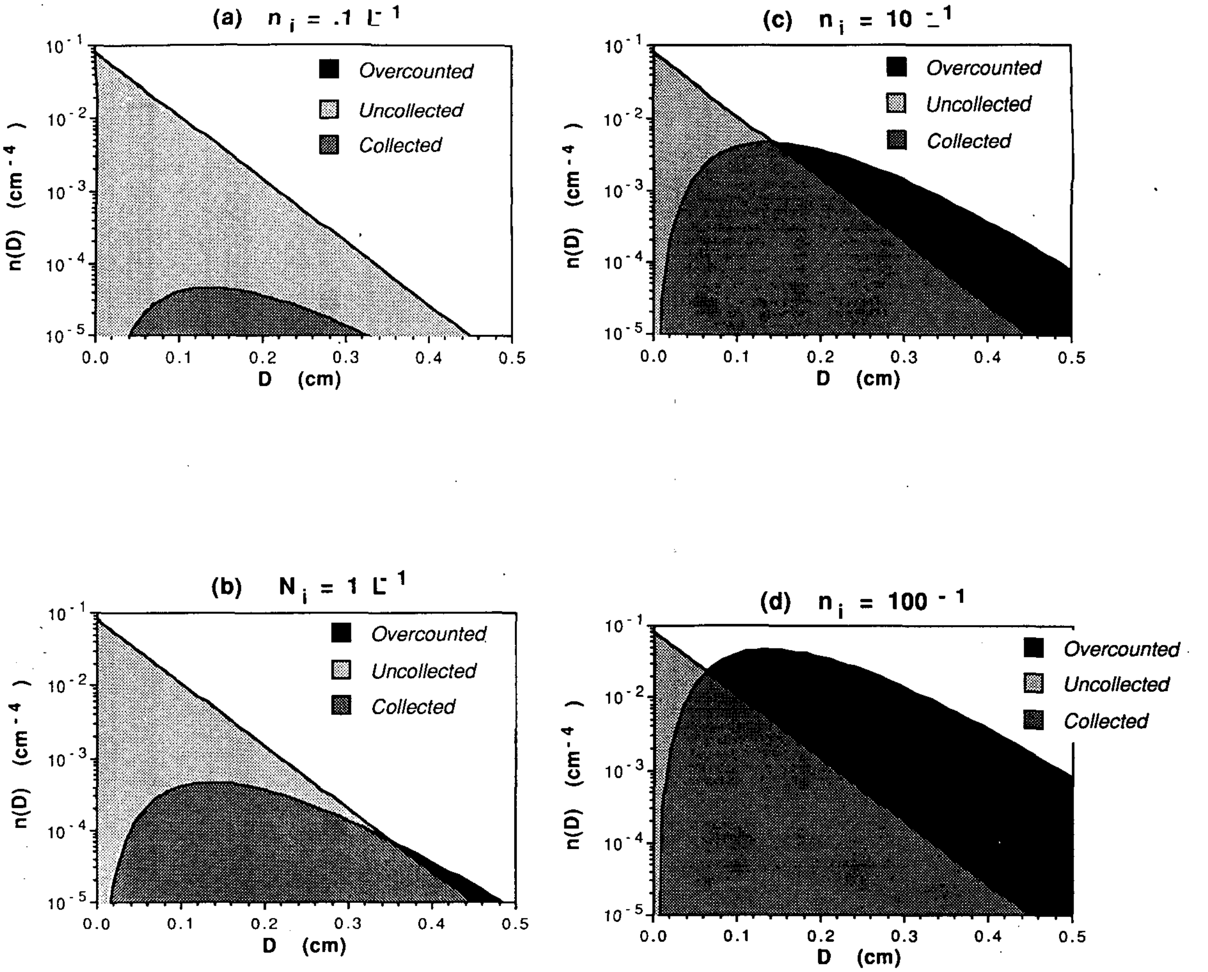

FIG. 1. The freezing of an exponential ($\alpha_r = 0$) raindrop size distribution with $n_{0r} = 0.08$ cm^{-4} and $\lambda_r = 20$ cm^{-1} resulting from the collection of small ice crystals is shown for ice number concentrations of (a) 0.1 L^{-1}, (b) 1 L^{-1}, (c) 10 L^{-1}, and (d) 100 L^{-1}. Light shading denotes those raindrops that do not collect any ice crystals; medium shading indicates those raindrops that do collect ice crystals, as properly represented by (4.19) and (4.23); and dark shading shows the overcounting of the larger raindrops, as represented by the traditional collection equations of (4.16) and (4.17). Calculations assume $E_{ri} = 1$, $\gamma = 1.2$, and $\Delta t = 10$ s. In (a) D_{rp} is not defined because $n_{ri} < 1$ for all drop sizes. Values of D_{rp} in (b)–(d) are 0.36 cm, 0.14 cm, and 0.06 cm, respectively.

$$\Delta q_z / q_z = \mathrm{QXACZ} \cdot \Delta t / q_z, \quad (4.18)$$

is much larger than one. Such conditions most often occur in association with collisional freezing of supercooled raindrops in convective cells. Although the temptation is to reduce each of the rates of the microphysical sink terms in proportion to the initial hydrometeor mixing ratio (q_z) as is done in other bulk parameterizations, this could result in unrealistically large microphysical rates and biases between different processes. This concern is especially important when partitioning the mass and number concentrations associated with the freezing of raindrops into various classes of precipitation ice.

Consider the mixing ratio of rain frozen in time step Δt due to collection of small ice (Δq_r),

$$\Delta q_r = \rho^{-1} \int_0^\infty m_r(D_r) P_{ri}(D_r) n_r(D_r) dD_r, \quad (4.19)$$

where $m_r(D_r) = \pi/6 \rho_L D_r^3$ is the mass of a spherical raindrop, $n_r(D_r)$ is the drop size distribution given by (3.2), $P_{ri}(D_r)$ is the probability function for drop freezing,

$$P_{ri}(D_r) = \min[1, n_{ri}(n_i, D_r)], \quad (4.20)$$

and

$$n_{ri}(n_i, D_r) = \pi/4 E_{ri} n_i D_r^2 V_r \Delta t \quad (4.21)$$

is the number of ice crystals collected by a drop. The assumption used to derive (4.16) is that a drop collects at most one ice crystal during the time step. However,

n_{ri} increases rapidly with drop size, such that drops larger than D_{rp} will collect more than one ice crystal [i.e., $n_{ri}(n_i, D_{rp}) = 1$] given that a sufficient number of ice particles are present. Figure 1 shows what portion of a raindrop distribution is frozen due to collection of small ice crystals, as well as how more drops are overcounted using (4.16) and (4.17) as the ice crystal number concentrations increase. Although there is no difference in calculating the rate of drop freezing using QIACR in (4.16) or $\Delta q_r/\Delta t$ in (4.19) when the ice crystal concentrations are small (Fig. 1a), the error associated with (4.16) increases dramatically with higher ice particle concentrations as the threshold drop size D_{rp} decreases; that is, more of the larger drops are overcounted as a result of each drop collecting more than one ice crystal during the time step (Figs. 1b–d). Detailed calculations indicate that the relative error associated with (4.16) is less than 5%–10% for values of ΔQ_{IACR} ($=\mathrm{QIACR}\cdot\Delta t/q_r$) less than 0.1, whereas essentially all of the rain is frozen when values of ΔQ_{IACR} exceed 7.5 for $\alpha_r = 0$ rain distributions and 5.0 for the $\alpha_r = 2.5$ rain distributions of Willis (1984); only for intermediate values of ΔQ_{IACR} are revised calculations of QIACR made using (4.19). Thus, final values for QIACR are

$$\mathrm{QIACR} = \begin{cases} \mathrm{QIACR\ from\ (4.16)}, & \Delta Q_{\mathrm{IACR}} < 0.1 \\ q_r/\Delta t, & \Delta Q_{\mathrm{IACR}} > 5\ (\alpha_r = 2.5) \\ & \quad \mathrm{or}\quad 7.5\ (\alpha_r = 0) \\ \Delta q_r/\Delta t\ \mathrm{from\ (4.19)}, & \mathrm{otherwise.} \end{cases} \tag{4.22}$$

A procedure similar to (4.22) is used to calculate final values for NIACR using either (4.17) or $\Delta n_r/\Delta t$, where

$$\Delta n_r = n_{or}\int_0^\infty \min\left(1, \frac{\pi}{4}E_{ri}n_iV_rD_r^2\Delta t\right)D_r^{\alpha_r}e^{-\lambda_rD_r}dD_r \tag{4.23}$$

is obtained from (3.2), (4.20), and (4.21).

When large collection rates occur between precipitation species, then the mass of species Z collected by species X in time step Δt is

$$\Delta q_z = \frac{\pi\rho_z}{6\rho}n_{oz}\int_0^\infty P_{xz}(D_z)D_z^{3+\alpha_z}e^{-\lambda_zD_z}dD_z, \tag{4.24}$$

$$P_{xz}(D_z) = \min[1, n_{xz}(n_{ox}, \lambda_x, D_z)], \tag{4.25}$$

$$n_{xz}(n_{ox}, \lambda_x, D_z) = \frac{\pi}{4}\gamma\Delta t n_{ox}\int_0^\infty E_{xz}(D_z + D_x)^2 \times |V_z - V_x|D_x^{\alpha_x}e^{-\lambda_xD_x}dD_x, \tag{4.26}$$

where E_{xz} is the collection efficiency, and n_{xz} is the number of particles of size D_z collected by species X. Numerical integration of (4.24) is performed only if the values of $\mathrm{QXACZ}\cdot\Delta t/q_z$ are in the ranges of 0.1–7.5 for the collection of $\alpha_r = 0$ distributed drops, 0.3–5.0 for the collection of $\alpha_r = 2.5$ distributed drops, and 0.5–1.5 for the collection of snow and graupel ($\alpha_s = \alpha_g = 0$). A final value for NXACZ is obtained by replacing $P_{ri}(D_r)$ in (4.23) with $P_{xz}(D_z)$. In situations where the freezing of rain by QXACR is modified using (4.24), the rates associated with three-body drop-freezing processes (QXACRY) are adjusted in order to satisfy (4.14) and (4.15).

In the future it should be possible to store numerical solutions for (4.19) and (4.24) in additional lookup tables by scaling the modified collection kernels based on the number concentrations of the collector particles. Successfully developing such a technique would make the microphysical scheme more computationally efficient.

b. *Conversion by riming processes (QXACWX, QXACWY, QWACXY, NWACXY)*

In the RH scheme and in the modification of the LFO scheme by Farley et al. (1989), snow can be converted to graupel (RH) or hail (LFO) by rapid cloud water riming when the mixing ratios of snow and cloud water exceed independently specified thresholds. Nevertheless, conversion from one ice class to another should be based upon changes in the bulk densities of the rimed particles. Because rime density is a complex function of the cloud droplet size, the ice particle surface temperature, and the impact velocity of the droplets onto the ice particle (Macklin 1962; Pflaum and Pruppacher 1979; Heymsfield and Pflaum 1985), the density characteristics of particles produced from the simplified riming conversion processes in RH and Farley et al. (1989) can differ substantially from rimed ice in real clouds. The effects of variable ice particle densities resulting from accretion of low-density rime upon the microphysical structure of a hailstorm has been studied by Farley (1987) using the explicit model of Farley and Orville (1986) with 20 size categories of precipitation ice.

In the current scheme, conversion between precipitation ice categories is based upon the riming rate and the rime density collected on the ice particles. Conversion by riming can occur from snow into graupel (QSACWG, QWACSG, NWACSG), from graupel into frozen drops/hail (QGACWH, QWACGH, NWACGH), and from frozen drops/hail into graupel (QHACWG, QWACHG, NWACHG); conversion from graupel into snow is not considered because the bulk characteristics of graupel remain essentially unchanged even when rapidly accreting low-density rime (Buser and Aufdermaur 1973; Farley 1987). For riming conversion to occur, it is assumed that 1) the rime density is similar to that of the converted particle species, and 2) a sufficient amount of rime has accumulated so as to alter the bulk density of the converted particles. The riming rates onto the converted and unconverted ice, respectively, are

$$\mathrm{QXACWY} = \mathrm{QXACW}[\gamma^*(3 + \alpha_x + b_x, \lambda_x D_{2xy}) - \gamma^*(3 + \alpha_x + b_x, \lambda_x D_{1xy})], \quad (4.27)$$

$$\mathrm{QXACWX} = \mathrm{QXACW} - \mathrm{QXACWY}, \quad (4.28)$$

where QXACW is given by (B.7). Diameter D_{1xy} is the minimum size in which the rime density is similar to that of the converted particle species, while D_{2xy} is the size in which the particle mass doubles within time interval Δt_{rime} (typically assumed to be 120 s), such that only the smaller particles ($D_x \leqslant D_{2xy}$) are considered to have had their densities sufficiently modified. Rime collected on ice particles smaller than D_{1xy} and larger than D_{2xy} remains a mass source for the rimed species X in (4.27), while in (4.28) rime collected on particles in the size range $D_{1xy} \leqslant D \leqslant D_{2xy}$ is a source of mass for the converted species Y. The rate at which rimed hydrometeors are converted from species X to species Y is given by

$$\mathrm{QWACXY} = q_x/(\Delta t)_{\mathrm{rime}}[\gamma^*(1 + \alpha_x + d_x, \lambda_x D_{2xy}) - \gamma^*(1 + \alpha_x + d_x, \lambda_x D_{1xy})], \quad (4.29)$$

$$\mathrm{NWACXY} = n_x/(\Delta t)_{\mathrm{rime}}[\gamma^*(1 + \alpha_x, \lambda_x D_{2xy}) - \gamma^*(1 + \alpha_x, \lambda_x D_{1xy})]. \quad (4.30)$$

The methods used to calculate D_{1xy} and D_{2xy} are presented in appendix B.

c. *Freezing and melting of precipitation ice (QXFM), shedding of liquid water (QXSHD, NXSHD)*

Liquid water is shed as a result of the complete melting of precipitation, or in order to maintain a maximum mass fraction of liquid water on the ice particle of F_{wm}. The value of F_{wm} is typically set to 0.5, which assumes that at most half of the mass of an ice particle is composed of liquid water. The number concentrations of precipitation ice change only when liquid water is shed due to the complete melting of ice particles, where it is assumed that the slopes of the particle distributions (λ_x) are approximately constant during this process (Koenig and Murray 1976; Kopp et al. 1983; Murakami 1990). The processes associated with the shedding of liquid water, as well as the rates of freezing and melting of precipitation ice, are described in appendix B.

Alternative methods for calculating changes in ice number concentrations by melting were also examined. First, the intercept of the particle distribution (n_{0x}) was assumed constant during melting, as in LFO and RH. But as Orville and Kopp (1977) and Kopp et al. (1983) noted, this method produced unrealistically large decreases in the ratio of large to small particle sizes, resulting in much larger melting rates than are represented in the current approach. A more sophisticated technique was then tested where the mass and number concentrations associated with only those smallest ice particles that melt completely within a *time step* were removed. Since exponential distribution for ice is usually assumed, this method worked in the opposite sense to the constant n_{ox} approach by removing many more of the smaller particles than the larger particles, resulting in unrealistically large mean particle diameters below the melting level with substantially smaller melting rates than in the constant λ_x approach. These different treatments of melting will be shown in future studies to have a strong impact upon how far the ice falls below the melting level.

d. *Initiation of small ice crystals*

There are four different modes by which ice crystals can be initiated in the model: deposition/condensation freezing, stochastic/homogeneous freezing of cloud droplets, ice multiplication by rime splintering (e.g., Hallett and Mossop 1974), and the less understood ice enhancement mechanism of Hobbs and Rangno (1985).

1) DEPOSITION/CONDENSATION FREEZING (QINT, NINT)

The nucleation of small ice crystals at temperatures warmer than −5°C follows COT and Murakami (1990), while at colder temperatures nucleation by deposition and condensation freezing following Meyers et al. (1992) was used:

$$\mathrm{NINT} = \max(0, w)\cdot\partial n_{in}/\partial z, \quad (4.31)$$

$$\mathrm{QINT} = \rho^{-1} m_{i0}\mathrm{NINT}, \quad (4.32)$$

$$n_{in} = \begin{cases} n_{in1}, & T_c \geqslant -5°\mathrm{C} \\ n_{in2}, & T_c < -5°\mathrm{C}, \end{cases} \quad (4.33)$$

$$n_{in1} = n_{io1}[(q_v - q_{is})/(q_{ws} - q_{is})]^{\alpha_1}\exp(-\beta_1 T_c), \quad (4.34)$$

$$n_{in2} = n_{io2}\exp(\alpha_2 \mathrm{SS}_i - \beta_2), \quad (4.35)$$

where w is the vertical velocity, m_{io} is the mass of a nucleated ice crystal (assumed to have an initial diameter of 25 μm), q_{is} and q_{ws} are the saturation mixing ratios with respect to ice and water, respectively, $\mathrm{SS}_i = q_v/q_{is} - 1$ is the supersaturation ratio with respect to ice, $n_{io2} = 10^{-3}$ cm^{-3}, $\alpha_2 = 12.96$, $\beta_2 = 0.639$ (Meyers et al. 1992), $\alpha_1 = 4.5$, $\beta_1 = 0.6$ K^{-1} (COT), and $n_{io1} = 5 \times 10^{-5}$ cm^{-3} in order for $n_{in1} = n_{in2}$ at −5°C. As in Meyers et al. (1992), n_{io1} can also be set to zero in order to prevent nucleation by deposition/sorption of ice crystals at temperatures warmer than −5°C. Following Ziegler (1985) and Murakami (1990), the rate of nucleation in (4.31) is assumed to be dominated by vertical advection. Meyers et al. (1992) formulated their scheme based upon improved measurements of crystal concentrations using continuous flow devices, which were available only at temperature above −25°C. The importance of ice initiation in the upper portions of convective systems supports an obvious need for ice particle and aerosol measurements at much colder temperatures (and higher altitudes).

2) FREEZING OF CLOUD WATER AND MELTING OF CLOUD ICE (QIFM, NIFM)

Murakami (1990) modified Wisner et al.'s (1972) probabilistic drop-freezing scheme in order to calculate the rate at which cloud droplets freeze stochastically. Probabilistic freezing of raindrops is not considered in this scheme because it is typically several orders of magnitude smaller than collisional drop freezing. A similar approach is adopted here by integrating Eq. (27) in Wisner et al. (1972) over the assumed droplet size distribution of (3.1), yielding

$$\mathrm{NIFM} = \int_0^\infty B'[\exp(A'T_c) - 1]\, v n(v) dv, \qquad (4.36)$$

$$\mathrm{QIFM} = \rho^{-1} \int_0^\infty B'[\exp(A'T_c) - 1] \rho_L v^2 n(v) dv. \qquad (4.37)$$

The droplet number concentration is assumed constant, except when the mean droplet diameter (D_w) reaches a minimum value ($D_{w\min}$), after which n_w changes so as to maintain a mean droplet diameter of $D_{w\min}$. This constraint prevents unrealistically small mean droplet sizes from developing in regions where many of the cloud droplets are removed by riming onto ice rather than evaporation into dry air. Otherwise, assuming a constant droplet number concentration produces mean droplet sizes that are small enough to inhibit the stochastic freezing of cloud droplets at cold temperatures ($T_c < -20$°C) where it is expected to be most effective. Using the definition for the mean droplet volume, the rate that droplets freeze into ice crystals at temperatures warmer than homogeneous freezing ($T_c > T_{\mathrm{hom}}$) is

$$\mathrm{QIFM} = \frac{2B'}{\rho_L n_w}[\exp(A'T_c) - 1]\rho q_w^2, \qquad (4.38)$$

$$\mathrm{NIFM}^* = \rho_L^{-1} B'[\exp(A'T_c) - 1]\rho q_w, \qquad (4.39)$$

$$\mathrm{NIFM} = \min[\mathrm{NIFM}^*, n_w/Dt]. \qquad (4.40)$$

The rate of cloud water freezing for $T_c \leqslant T_{\mathrm{hom}}$ is

$$\mathrm{QIFM} = \max(0, q_w/\Delta t + \mathrm{QCND}), \qquad (4.41)$$

$$\mathrm{NIFM}^* = \rho_L^{-1} B'[\exp(A'T_c) - 1]\mathrm{QIFM}\cdot\Delta t, \qquad (4.42)$$

and NIFM is given by (4.40). The rates of droplet freezing given by (4.38)–(4.40) increase rapidly as temperatures decrease toward T_{hom}, such that droplets typically glaciate completely within ±5°C of T_{hom} (assumed to be −40°C). Although (4.41)–(4.42) are used to ensure that homogeneous glaciation will occur when $T_c \leqslant T_{\mathrm{hom}}$, it may soon be possible to improve upon this parameterization of homogeneous droplet freezing (Cotton 1993, personal communication).

Melting of small ice crystals is assumed to proceed rapidly, such that

$$\mathrm{QIFM} = -q_i/\Delta t, \qquad (4.43)$$

$$\mathrm{NIFM} = -n_i/\Delta t. \qquad (4.44)$$

3) RIME-SPLINTERING ICE MULTIPLICATION (QIHMX, NIHMX)

Rime splintering has been hypothesized to be an important secondary ice multiplication process in convective clouds (Hallett and Mossop 1974; Mossop 1976; Hallett et al. 1978; Black and Hallett 1986; Willis and Hallett 1991; Houze et al. 1992). Although the mechanism was parameterized in COT and Ziegler (1988), a thorough investigation of the process was undertaken in this study using the recent laboratory results of Mossop (1985). The number of ice splinters produced depends upon 1) the ratio of small (≤12 μm) to large (≥25 μm) cloud droplets rimed onto the ice particle, 2) the cloud temperature between −2°C and −8°C, and 3) the fall speeds of ice particles less than 6 m s^{-1}. A general derivation of rime splintering by precipitation ice is described in appendix B. Rime splintering will be shown in future studies to be effective in increasing the ice concentrations in late-mature and dissipating convective cells. It may also be important in weak convective clouds, in convective elements embedded within stratiform clouds, and in storms where rimed particles are recycled into updrafts with high water contents.

4) ICE ENHANCEMENT (QIHR, NIHR)

Large number concentrations of small ice particles in maritime clouds have been observed to occur in a two-step process: 1) frozen and unfrozen drops form in concentrations of a few per liter near cloud top, followed within 5–10 min by 2) the onset of small, uniformly sized vapor-grown ice crystals in concentrations of 10–100 L^{-1} (Hobbs and Rangno 1985, 1990; Rangno and Hobbs 1991). This ice enhancement mechanism occurs in the upper regions of clouds that have cloud-top temperatures colder than −6°C, are wider than 3 km in diameter, and have a broad droplet spectrum. Recently, Barth et al. (1992) prescribed the effects of ice enhancement in their study of the chemistry of rainbands. An independently derived representation of Hobbs and Rangno's aircraft observations is presented in appendix B for the purpose of evaluating its impact upon model simulations of convective systems in different large-scale environments, even though the underlying physical processes associated with these observations are not well understood.

e. Adjustment of deposition rates

All microphysical processes involving the exchange of water vapor between various hydrometeor constituents and the environment (i.e., QXEVP, QXDEP, QCND, QIDEP, and QINT) are calculated independently in the current scheme. But as in real clouds, competition between these different processes for the available water vapor supply occurs in the mixed-phase region of a cloud where large numbers of ice particles coexist with cloud droplets. Constraints must be placed on these microphysical processes in order to prevent too much drying (moistening) of the cloud by condensation (evaporation) and deposition (sublimation). In some microphysical models, this problem is overcome through the use of saturation adjustment schemes, which assume that 1) the saturation vapor mixing ratio varies between water and ice saturation in proportion to the relative amount of cloud water and cloud ice, 2) the relative rates of cloud water condensation and cloud ice deposition are a linear function of cloud temperature (e.g., Lord et al. 1984; Tao et al. 1989).

A less restrictive technique is used in the current scheme that adjusts the rates of vapor deposition onto ice only when too much water vapor is removed from (added to) the environment in association with large condensation (evaporation) and deposition (sublimation) rates. It is implemented if 1) $q_v < q_{is}$ due to ice deposition and cloud water condensation at $T_c > T_{\rm hom}$ ($T_{\rm hom}$ is the homogeneous freezing temperature of $-40°$C), 2) $q_v > q_{is}$ as a result of ice sublimation and cloud water evaporation at $T_c > T_{\rm hom}$, or 3) ice deposition occurred at $T_c \leqslant T_{\rm hom}$. The procedure assumes that cloud water condensation is a much more rapid process than deposition onto ice at $T_{\rm hom} < T_c < 0°$C. Representing the change in water vapor mixing ratio resulting from net condensation and net deposition processes, respectively, by

$$\mathrm{CND} = \Delta t(\mathrm{QCND} + \mathrm{QREVP}) \qquad (4.45)$$

and

$$\mathrm{DEP} = \Delta t(\mathrm{QINT} + \mathrm{QIDEP} + \mathrm{QSDEP} + \mathrm{QGDEP} + \mathrm{QHDEP}), \qquad (4.46)$$

then the change in the water vapor mixing ratio is

$$q_v^{t+\Delta t} = q_{is}^{t+\Delta t} = q_v - \mathrm{CND} - \zeta\mathrm{DEP}, \qquad (4.47)$$

where ζ is a coefficient ($0 \leqslant \zeta \leqslant 1$) used to adjust the various ice deposition rates in (4.46) so that the final water vapor mixing ratio at time $t + \Delta t$ is at ice saturation (QCND, QREVP, and QXDEP are defined in appendix B). The saturation vapor mixing ratio with respect to ice at time $t + \Delta t$ is

$$q_{is}^{t+\Delta t} = q_{is}[1 + a_2\Delta T/(T - 7.66)^2], \qquad (4.48)$$

where T is the air temperature (deg K) and $a_2 = 5807.7$ (Tao et al. 1989), and the change in temperature due to latent heating is

$$\Delta T = (L_f\Delta t\mathrm{QIFM} + L_v\mathrm{CND} + \zeta\cdot L_s\mathrm{DEP})/C_p. \qquad (4.49)$$

The rate of freezing of cloud droplets into small ice crystals (QIFM) is included in the latent heating calculation because it can be substantial at colder temperatures. Combining (4.47)–(4.49) yields an expression for the coefficient ζ used to modify each of the deposition processes in (4.46),

$$\zeta = \frac{q_v - \mathrm{CND} - q_{is}\left[1 + \dfrac{a_2(L_f\Delta t\mathrm{QIFM} + L_v\mathrm{CND})}{C_p(T-7.66)^2}\right]}{\mathrm{DEP}\left[1 + \dfrac{a_2L_sq_{is}}{C_p(T-7.66)^2}\right]}. \qquad (4.50)$$

This method of constraining only the rates of vapor deposition has advantages over the adjustment techniques used in other microphysical parameterizations. In the proposed method, water vapor mixing ratios in convective updrafts are near water saturation in the presence of cloud water. Larger deposition rates onto ice reduce the supply of water vapor available for condensation onto the cloud droplets as ice concentrations increase with height (decreasing temperature), while at the same time cloud water is being removed rapidly by riming onto the various ice hydrometeors. Eventually enough ice is present to absorb the excess water vapor provided by ascent in the updrafts, such that water vapor mixing ratios fail to reach water saturation and prevent the condensation of cloud water. Because ice grows at the expense of the cloud water in this ice scheme, there is no need for parameterizing the Beregeron–Findeisen process as in LFO and RH. Furthermore, these competitive rates will vary in a dynamically and microphysically consistent manner in response to changes made to the processes parameterized in the scheme (this is also a feature of the COT scheme). This consideration is important when assessing the impact of microphysical sensitivity tests.

f. Conversion of small ice to snow (QICNVS, NICNV, NSCNV)

Small ice crystals are converted into snow as they grow to large enough sizes by deposition and aggregation. An initial technique was adopted that gradually converted the mass and number concentrations of ice crystals larger than a maximum size $D_{i\max}$ (typically 0.05 cm) into snow over a time interval Δt_{is} (varied between 60 and 300 s), such that

$$\mathrm{QICNVS} = (q_i/\Delta t_{is})[1 - \gamma^*(\alpha_i + d_i + 1, \lambda D_{i\max})], \qquad (4.51)$$

$$\mathrm{NICNV} = \mathrm{NSCNV} = (n_i/\Delta t_{is})[1 - \gamma^*(\alpha_i + 1, \lambda D_{i\max})]. \qquad (4.52)$$

But after conducting numerous model simulations, it was discovered that this conversion method did not conserve the higher moments of the particle spectra, such that the combined radar reflectivities associated with the small ice and snow increased by as much as 10 dBZ as a result of applying (4.51) and (4.52).

An alternative parameterization was derived by 1) conserving radar reflectivity during the conversion process, 2) assuming the number concentrations of cloud ice are approximately constant by converting a few of the largest crystals into snow, and 3) converting from cloud ice to snow by adjusting the slope of the cloud ice distribution (λ_i) to a minimum value λ_{i0} (50 cm^{-1}) only when $\lambda_i < \lambda_{i0}$. The resultant process for converting ice crystals into snow is

$$\text{QICNVS} = (q_i/\Delta t)[1 - (\lambda_i/\lambda_{i0})^3], \quad (4.53)$$

$$\text{NSCNV} = (n_i/\Delta t)[1 - (\lambda_i/\lambda_{i0})^3]/[1 + (\lambda_i/\lambda_{i0})^3] \quad (4.54)$$

and NICNV = 0.

5. Radar reflectivity

Because many studies have comprehensively documented, as a function of space and time, the radar structure of storms in different geographical regions, a reasonably straightforward and comprehensive means of evaluating model performance is to compare simulated and observed radar reflectivity fields. Since the microphysical parameterization allows for variable particle size distributions, as well as calculates the liquid water contents on precipitation ice, a simple method for calculating radar reflectivity using Rayleigh theory is described in appendix C. The approach of Smith et al. (1975) has been used in previous models to calculate the radar reflectivities associated with large, wet (hail) ice (e.g., Orville and Kopp 1977; Ziegler 1985; Banta and Hanson 1987; McCumber et al. 1991); however, these calculations were based on a very limited set of microphysical conditions, in which $n_{0h} = 0.0003$ cm^{-4} was assumed for the hail distribution with a constant water film 0.5 mm thick around the hail particles. Surprisingly, the reflectivities computed from (C.11) using the hail size spectra in Smith et al. (1975) are within ±0.5 dBZ of their Mie calculations for a 10-cm radar. Nevertheless, future plans are to improve the technique of calculating reflectivities using Mie scattering theory, since errors will increase for smaller-wavelength radars and for ice particles with more complicated ice–water topologies.

6. Issues regarding spectral characteristics of particle size distributions

The equations describing the rate of change of hydrometeor number concentrations due to accretion processes were derived based on conserving the number concentrations of the interacting species. At first this approach seemed straightforward and logical, and it is the physical assumption used to derive NRACXY and NXACRY in (4.12), NIACR in (4.17), NWACXY in (4.30), and NXACS in (B.3). However, GCE model simulations of GATE and TAMEX squall systems revealed that the simulated radar reflectivities in the convective cells above the freezing level were up to 10–15 dBZ higher than observed. Reflectivity maxima exceeded 60 dBZ in the modeled convective cores above the freezing level, which is inconsistent with GATE and TAMEX radar observations of modest peak reflectivities (50–55 dBZ) at lower levels with reflectivities decreasing steadily with height above the freezing level (Zisper and LeMone 1980; Szoke et al. 1986; Szoke and Zipser 1986; Jorgensen and LeMone 1989).

Figure 2 illustrates how the slopes (mean diameters) of the frozen drop spectra decrease (increase) dramatically with respect to the original drop size distributions when the mass and number concentrations of the collected drops in Fig. 1 are substituted into (3.3). This artificial decrease in the slopes of the converted particle spectra is especially large when few ice crystals are present (Figs. 2a and 2b), since, as Fig. 1 shows, only the largest raindrops are frozen [see also Eqs. (4.20) and (4.25)]. The significant increase in the number of particles larger than 4 mm in diameter (Figs. 2b–d) illustrates how the combined radar reflectivity factors (D^6 moment) of the parameterized particle distributions can increase substantially as a result of strictly conserving particle number concentrations in the conversion process, while at the same time constraining the particle distributions to remain exponential. Such redistribution of the particle spectra is clearly undesirable, especially since there is a much greater functional dependence of λ_x upon the microphysical rates than number concentration.

The size distributions of the collected drops shown in Fig. 1 exhibit a much larger degree of kurtosis than the exponential distribution associated with the original drop population, such that the spectra of the collected drops would be better represented by gamma distributions with large shape parameters ($\alpha_x \gg 0$). The errors in simulated radar reflectivities are due to the constraint of assuming constant shape parameters for each of the precipitation species during a model run. Conserving the number concentrations, mixing ratios, and radar reflectivities (D^6 moment) when converting from one precipitation category to another (e.g., the freezing of a few raindrops) requires calculating the variations in the slopes, intercepts, and shape parameters of the interacting particle distributions. Because the current scheme predicts variations in λ_x and n_{0x} for an assumed constant α_x, errors in reflectivity will occur when conserving the number concentrations and mass mixing ratios of the various precipitation categories. Calculating the changes in

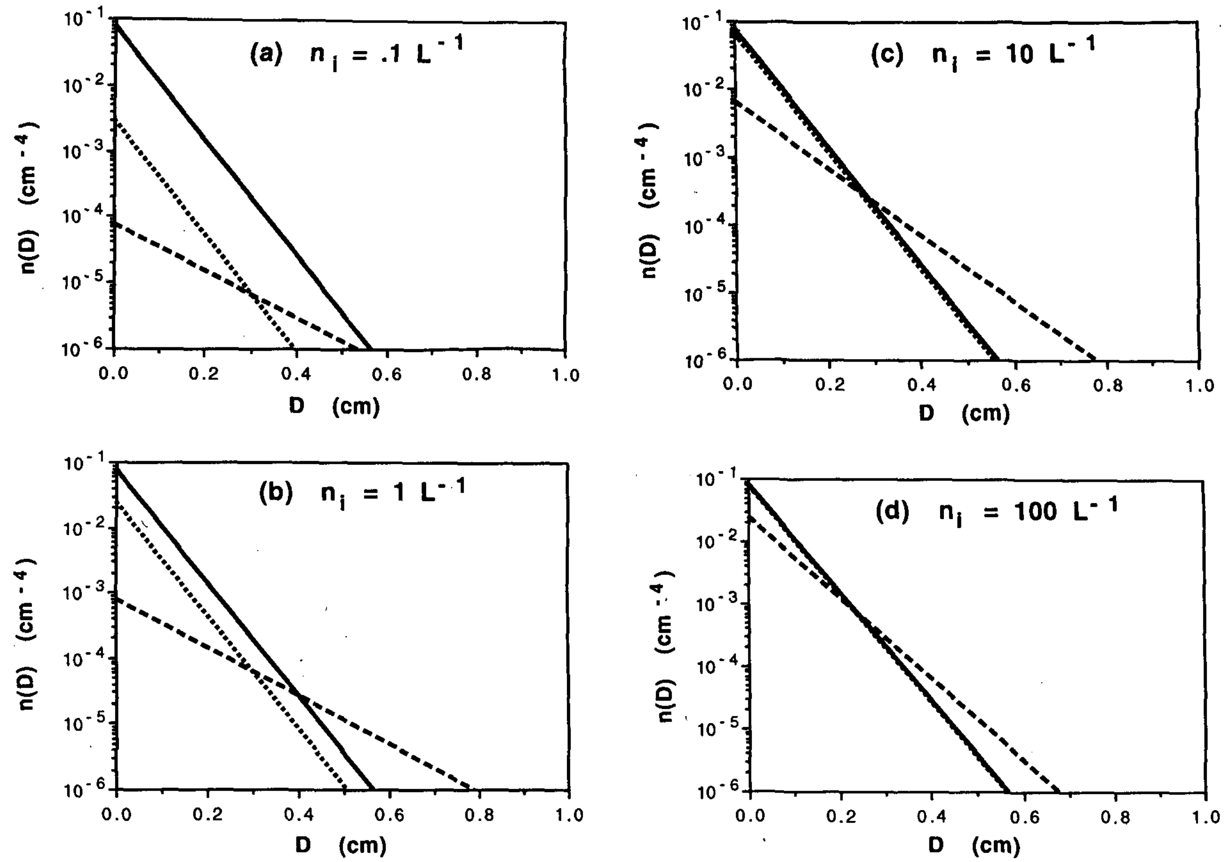

FIG. 2. The unfrozen raindrop size distribution (sum of the collected and uncollected drops) in Fig. 1 is shown by the solid lines in (a)–(d). The dashed lines represent the ($\alpha_x = 0$) size distributions of the water-equivalent ($\rho_x = \rho_L$) frozen drops associated with the number concentrations and mixing ratios of the collected drops in Fig. 1, where the radar reflectivity associated with the redistribution of collected and uncollected drops increased by (a) 1.8 dBZ, (b) 6.7 dBZ, (c) 6.7 dBZ, and (d) 3.7 dBZ. The dotted lines represent the size spectra of the water-equivalent frozen drops calculated by assuming the same slopes as for the original, unfrozen drop size distribution, in which the radar reflectivity associated with the redistribution of collected and uncollected drops increased by 0.01 dBZ in (a), decreased by 0.8 dBZ in (b), decreased by 0.6 dBZ in (c), and decreased by 0.08 dBZ in (d).

the shape parameters of different hydrometeor classes is beyond the scope of this paper, and the usefulness of such an endeavor will likely be determined in the future by advancements in computer technology and by improvements in explicit, detailed microphysical schemes.

Although some of the improved microphysical processes discussed in the previous section helped to reduce the large discrepancy between the simulated and observed radar fields, it is most important that *the spectral characteristics (i.e., λ_x) of the interacting particle distributions be preserved in the conversion process* rather than *strictly conserving the number concentrations of the constituent species.* This conclusion was also made in determining the final version of other microphysical processes described in section 4 and in appendix B (e.g., NXEVP, NXDEP, NXSHD, NSCNV). Figure 2 shows how the size distributions of the collected, frozen drops are improved by assuming the same slope as for the unfrozen rain.

Consequently, those microphysical processes that involve conversion between hydrometeor categories as a result of accretional processes have been rederived by conserving the slope for the particle distributions:

$$\mathrm{NXACI} = (n_i/q_i)\mathrm{QXACI}, \qquad (6.1)$$

$$\mathrm{NXACS} = (n_s/q_s)\mathrm{QXACS}, \qquad (6.2)$$

$$\mathrm{NWACXY} = (n_x/q_x)\mathrm{QWACXY}, \qquad (6.3)$$

$$\mathrm{NRACXY} = (n_x/q_x)\mathrm{QRACXY}, \qquad (6.4)$$

$$\mathrm{NIACR} = (R_Z \cdot n_r/q_r)\mathrm{QIACR}, \qquad (6.5)$$

$$\mathrm{NXACRY} = \frac{\left[\begin{array}{l}(R_z n_r/q_r)\mathrm{QXACRY}^2 \\ \qquad + (n_x/q_x)\mathrm{QRACXY}^2\end{array}\right]}{\mathrm{QXACRY} + \mathrm{QRACXY}}. \qquad (6.6)$$

The first four equations are similar to the relationships for NXDEP and NXEVP [see Eqs. (B.55) and (B.56), respectively]. Furthermore, many of the processes affecting ice number concentrations in the ice schemes of Koenig and Murray (1976) and Murakami (1990) have a similar functional form to (6.1)–(6.4). The last two equations differ in that these processes involve converting from raindrops, which may have an exponential ($\alpha_r = 0$) or gamma ($\alpha_r = 2.5$) distribution, to $\alpha_x = 0$ ice distributions. Appendix D contains a derivation for R_Z, which is a correction factor used to conserve the radar reflectivity factor when the shape parameter (α) changes from one particle distribution to another. For example, $R_Z = 1$ in (6.5) and (6.6) when the conversion process occurs between two exponential hydrometeor distributions (e.g., $\alpha_r = \alpha_x = 0$); however, when $\alpha_r = 2.5$ distributed raindrops freeze to form $\alpha_x = 0$ distributed ice, $R_Z = 4.181$ in order to conserve the D_m^6 moment of the particle distributions (D_m is the equivalent melted diameter of an ice particle, which has a mass equal to that of a raindrop of the same size). For the three-body accretion process in (6.6), an average of the λ associated with the colliding particle distributions is used that is weighted by their respective mass conversion rates (QXACRY for the freezing of drops; QRACXY for the accretion of q_x ice).

7. Conclusions

The following improvements have been made to the proposed bulk microphysical scheme in comparison to other bulk parameterizations:

- Four categories of ice are predicted in the model (small ice crystals, snow, graupel, *and* frozen drops/hail).
- Number concentrations of each ice class are predicted.
- The liquid water fraction is calculated for each of the precipitation ice species.
- Small ice crystals have a dispersive size distribution with nonzero terminal fall speeds.
- Improvements have also been made in parameterizing the accretion of precipitation, riming, conversion, raindrop freezing, and the freezing of liquid water on ice, ice multiplication and ice enhancement processes, aggregation of small ice crystals and snow, rates of cloud water condensation and ice deposition, and conversion processes between hydrometeor classes.

Calculating the number concentrations of the various ice categories offered unique problems that needed to be overcome in developing the parameterization. The most important problem that was addressed was how to formulate the conversion of particle number concentrations between hydrometeor species, where it was concluded that, in order to conserve the higher particle moments, preserving the slopes of the interacting particle distributions is more important than conserving the number concentrations of the particle species. A future study will assess the sensitivity of the simulated convection to different parameterized drop size distributions, terminal fall speeds, and aggregation efficiencies of ice crystals and snow, ice nucleation at cold temperatures ($T_c < -20°C$), changes in particle number concentrations due to melting and sublimation, and changes in hydrometeor concentrations associated with various conversion processes (including drop freezing and riming conversion) between hydrometeor species.

The double-moment four-class ice scheme has been developed to represent the microphysical structure of storms in different large-scale conditions. Given the current limitations in our knowledge of important characteristics of ice in clouds, it will be shown that the radar structure associated with the convective and stratiform portions of mesoscale convective systems in different environments are reproduced well with minimal tuning of the parameterization. Predicting the liquid water fraction on ice should also allow for improved calculations of active and passive radiometric signatures using linked cloud and radiation models.

The approach adopted in the current scheme has been to improve the parameterization of various accretion and rime conversion processes by storing the solutions to complex, nonanalytic equations in detailed lookup tables. In the future, additional lookup tables will be used extensively to represent many more of the microphysical processes using results from explicit warm rain (e.g., Clark 1973; Soong 1974; Young 1975; Kogan 1991) and ice phase parameterizations (Takahashi 1976; Hall 1980; Farley and Orville 1986), laboratory experiments, and future airborne microphysical observations, such as from TOGA COARE (Tropical Ocean Global Atmosphere Coupled Ocean–Atmosphere Response Experiment). It is envisioned that the current bulk parameterization can be made more realistic using results from detailed observational and theoretical studies, yet remain computationally efficient given the need for more physical processes to be included in numerical models, as well as the use of nested or adaptive grids in combined mesoscale–convective models.

Acknowledgments. The author gratefully acknowledges Drs. Joanne Simpson and Wei-Kuo Tao for their support and encouragement of this research, as well as their thoughtful review of the manuscript. Constructive comments from Drs. William Cotton, Richard Farley, and an anonymous reviewer are also appreciated. The author also thanks Dr. Harold Orville for finding inadequacies in the parameterization of melting ice (which have since been corrected) during his review of Part II. The author is also grateful to Drs. J. Theon and R. Kakar for their support of this study under Contract 460-23-54 of the NASA Headquarters Radiation, Dynamics and Hydrology Branch, and by the NASA TRMM project under Contract 460-63-58.

APPENDIX A

Continuity Equations

The prognostic equations for the mixing ratios of all phases of water in the parameterization (i.e., vapor, liquid, ice, and liquid water on ice) are as follows:

$$\frac{dq_v}{dt} = -\text{QCND} - \text{QREVP} - (1-\delta)(\text{QSEVP} + \text{QGEVP} + \text{QHEVP}) - \delta(\text{QINT} + \text{QIDEP} + \text{QSDEP} + \text{QGDEP} + \text{QHDEP}), \quad \text{(A.1)}$$

$$\frac{dq_w}{dt} = \text{QCND} - \text{QRAUT} - \text{QRACW} - \text{QSACWS} - \text{QGACWG} - \text{QHACWH} - \text{QIFM} - \delta(\text{QIACW} + \text{QIHR} + \text{QSACWG} + \text{QGACWH} + \text{QHACWG}), \quad \text{(A.2)}$$

$$\frac{dq_i}{dt} = \text{QIFM} + \delta(\text{QINT} + \text{QIDEP} + \text{QIACW} + \text{QIHR} + \text{QIHMS} + \text{QIHMG} + \text{QIHMH} - \text{QICNVS} - \text{QRACI} - \text{QSACI} - \text{QGACI} - \text{QHACI}), \quad \text{(A.3)}$$

$$\frac{dq_r}{dt} = \text{QREVP} + \text{QRAUT} + \text{QRACW} + \text{QSSHD} + \text{QGSHD} + \text{QHSHD} - \delta(\text{QIACR} + \text{QSACRS} + \text{QSACRG} + \text{QSACRH} + \text{QGACRG} + \text{QGACRH} + \text{QHACR}), \quad \text{(A.4)}$$

$$\frac{dq_s}{dt} = \text{QSACWS} - \text{QGACS} - \text{QHACS} - \text{QSSHD} + (1-\delta)\text{QSEVP} + \delta(\text{QSDEP} + \text{QICNVS} + \text{QSACI} + \text{QSACRS} - \text{QRACSG} - \text{QRACSH} - \text{QWACSG} - \text{QIHMS}), \quad \text{(A.5)}$$

$$\frac{dq_g}{dt} = \text{QGACWG} + \text{QGACS} - \text{QGSHD} + (1-\delta)\text{QGEVP} + \delta(\text{QGDEP} + \text{QGACI} + \text{QGACRG} + \text{QSACRG} + \text{QRACSG} + \text{QSACWG} + \text{QWACSG} + \text{QHACWG} + \text{QWACHG} - \text{QRACGH} - \text{QWACGH} - \text{QIHMG}), \quad \text{(A.6)}$$

$$\frac{dq_h}{dt} = \text{QHACWH} + \text{QHACS} - \text{QHSHD} + (1-\delta)\text{QHEVP} + \delta(\text{QHDEP} + \text{QHACI} + \text{QHACR} + \text{QIACR} + \text{QRACI} + \text{QSACRH} + \text{QRACSH} + \text{QGACRH} + \text{QRACGH} + \text{QGACWH} + \text{QWACGH} - \text{QWACHG} - \text{QIHMH}), \quad \text{(A.7)}$$

$$\frac{dq_{sw}}{dt} = \text{QSACW} - \text{QSFM} - \text{QSSHD} - F_{sw}(\text{QGACS} + \text{QHACS}) + (1-\delta)\text{QSEVP} + \delta[\text{QSACRS} - F_{sw}(\text{QRACSG} + \text{QRACSH} + \text{QWACSG})], \quad \text{(A.8)}$$

$$\frac{dq_{gw}}{dt} = \text{QGACW} - \text{QGFM} - \text{QGSHD} + F_{sw}\cdot\text{QGACS} + (1-\delta)\text{QGEVP} + \delta[\text{QGACRG} + \text{QSACRG} + \text{QSACWG} + \text{QHACWG} + F_{sw}(\text{QRACSG} + \text{QWACSG}) + F_{hw}\cdot\text{QWACHG} - F_{gw}(\text{QRACGH} + \text{QWACGH})], \quad \text{(A.9)}$$

$$\frac{dq_{hw}}{dt} = \text{QHACW} - \text{QHFM} - \text{QHSHD} + F_{sw}\cdot\text{QHACS} + (1-\delta)\text{QHEVP} + \delta[\text{QIACR} + \text{QSACRH} + \text{QGACRH} + \text{QHACR} + \text{QGACWH} + F_{sw}\cdot\text{QRACSH} + F_{gw}(\text{QRACGH} + \text{QWACGH}) - F_{hw}\cdot\text{QWACHG}]. \quad \text{(A.10)}$$

The functions δ in (A.1)–(A.10) and F_{xw} in (A.8)–(A.10) are defined as

$$\delta = \begin{cases} 1, & T < 0°\mathrm{C} \\ 0, & \text{otherwise}, \end{cases} \quad (A.11)$$

$$F_{xw} = q_{xw}/q_x, \quad (A.12)$$

where the variable x represents the precipitation ice species of snow, graupel, and hail/frozen drops ($x = s, g, h$).

Changes in the simulated potential temperature (q) due to latent heating are calculated using the following thermodynamic energy equation:

$$\frac{d\theta}{dt} = \frac{L_v}{\Pi C_p}(\mathrm{QCND} + \mathrm{QREVP}) + \frac{\delta L_s}{\Pi C_p}(\mathrm{QINT} + \mathrm{QIDEP} + \mathrm{QSDEP} + \mathrm{QGDEP} + \mathrm{QHDEP}) + \frac{L_f}{\Pi C_p}[\mathrm{QIFM} + \mathrm{QSFM} + \mathrm{QGFM} + \mathrm{QHFM} + \delta(\mathrm{QIACW} + \mathrm{QIHR})], \quad (A.13)$$

where Π is the Exner function $(p_0/p)^\kappa$ and $\kappa = R_d/C_p$.

Finally, prognostic equations for the number concentrations of each ice species are

$$\frac{dn_i}{dt} = \mathrm{NIFM} + \delta(\mathrm{NINT} + \mathrm{NIDEP} + \mathrm{NIHMS} + \mathrm{NIHMG} + \mathrm{NIHMH} + \mathrm{NIHR} - \mathrm{NICNV} - \mathrm{NIACI} - \mathrm{NRACI} - \mathrm{NSACI} - \mathrm{NGACI} - \mathrm{NHACI}), \quad (A.14)$$

$$\frac{dn_s}{dt} = \mathrm{NSBR} - \mathrm{NSACS} - \mathrm{NGACS} - \mathrm{NHACS} + (1-\delta)(\mathrm{NSEVP} - \mathrm{NSSHD}) + \delta(\mathrm{NSCNV} + \mathrm{NSDEP} - \mathrm{NRACSG} - \mathrm{NRACSH} - \mathrm{NWACSG}), \quad (A.15)$$

$$\frac{dn_g}{dt} = (1-\delta)(\mathrm{NGEVP} - \mathrm{NGSHD}) + \delta(\mathrm{NGDEP} + \mathrm{NSACRG} + \mathrm{NWACSG} + \mathrm{NWACHG} - \mathrm{NRACGH} - \mathrm{NWACGH}), \quad (A.16)$$

$$\frac{dn_h}{dt} = (1-\delta)(\mathrm{NHEVP} - \mathrm{NHSHD}) + \delta(\mathrm{NHDEP} + \mathrm{NIACR} + \mathrm{NSACRH} + \mathrm{NGACRH} + \mathrm{NWACGH} - \mathrm{NWACH}). \quad (A.17)$$

APPENDIX B

Description of Microphysical Processes

a. Collection of snow (QXACS, NXACS)

Letting D_{xw} represent the minimum particle diameter in which the collector particles (i.e., graupel and frozen drops) become wet, such that only those collector particles larger than D_{xw} are wet ($D \geqslant D_{xw}$), the resulting collection kernel is

$$\mathrm{QXACS} = \frac{\pi}{4\rho} c_s n_{ox} n_{oz} \Lambda_q \Delta V_q [(E_{xs})_{\mathrm{dry}}(1 - \mathrm{FQ}_{xs}) + (E_{xs})_{\mathrm{wet}}\mathrm{FQ}_{xs}], \quad (B.1)$$

where Λ_q and ΔV_q are described in (4.3)–(4.4), $(E_{xs})_{\mathrm{dry}}$ and $(E_{xs})_{\mathrm{wet}}$ represent the collection efficiencies of snow for dry and wet collector (i.e., graupel or frozen drop) particles, respectively [see Eq. (B.12) for values of $(E_{xs})_{\mathrm{dry}}$ and $(E_{xs})_{\mathrm{wet}}$], and

$$FQ_{xs} = \frac{\int_{D_{xw}}^{\infty} D_x^{\alpha_x} e^{-\lambda_x D_x} dD_x \int_0^{\infty} (D_x + D_s)^2 \times |V_x - V_s| D_s^{\alpha_s + d_s} e^{-\lambda_s D_s} dD_s}{\int_0^{\infty} D_x^{\alpha_x} e^{-\lambda_x D_x} dD_x \int_0^{\infty} (D_x + D_s)^2 \times |V_x - V_s| D_s^{\alpha_s + d_s} e^{-\lambda_s D_s} dD_s}, \quad (B.2)$$

is the fractional contribution to the collection kernel made by the wet collector particles. The diameter D_{xw} is calculated using a heat balance equation similar to Musil (1970). Since $D_{xw} = 0$ and $\mathrm{FQ}_{xs} = 1$ at $T_c \geqslant 0°\mathrm{C}$, QXACS is calculated from (4.2) with $(E_{xs})_{\mathrm{wet}}$ as the collection efficiency of snow. Three-dimensional lookup tables for FQ_{xs} (i.e., FQ_{gs} for QGACS and FQ_{hs} for QHACS) were created in the same manner as for ΔV_q using the same values of $(\lambda_x)_j$ as in Table 4; however, ten discrete, logarithmically spaced values of $(D_{xw})_j$ from 0.05 to 1.0 cm and only five logarithmically spaced values of $(\lambda_s)_j$ from 10 cm^{-1} to 100 cm^{-1} are needed in the FQ_{xs} table.

Tables of ΔV_n and FN_{xs} were also created for the purposes of calculating the changes in the number concentrations of collected snow (NGACS, NHACS), where

$$\mathrm{NXACS} = \frac{\pi}{4} n_{ox} n_{oz} \cdot \Lambda_n(\lambda_x, \lambda_s) \cdot \Delta V_n(\lambda_x, \lambda_s)[(E_{xs})_{\mathrm{dry}}(1 - \mathrm{FN}_{xs}) + (E_{xs})_{\mathrm{wet}} \mathrm{FN}_{xs}], \tag{B.3}$$

$$\Lambda_n = \Lambda_n(\lambda_x, \lambda_s) = \frac{\Gamma(3+\alpha_x)\Gamma(1+\alpha_s)}{\lambda_x^{3+\alpha_x}\lambda_s^{1+\alpha_s}} + 2\frac{\Gamma(2+\alpha_x)\Gamma(2+\alpha_s)}{\lambda_x^{2+\alpha_x}\lambda_s^{2+\alpha_s}} + \frac{\Gamma(1+\alpha_x)\Gamma(3+\alpha_s)}{\lambda_x^{1+\alpha_x}\lambda_s^{3+\alpha_s}}, \tag{B.4}$$

$$\Delta V_n = \Delta V_n(\lambda_x, \lambda_s) = \Lambda_n^{-1} \int_{D_{xw}}^{\infty} D_x^{\alpha_x} e^{-\lambda_x D_x} dD_x \int_0^{\infty} (D_x + D_s)^2 |V_x - V_s| D_s^{\alpha_s} e^{-\lambda_s D_s} dD_s, \tag{B.5}$$

and

$$\mathrm{FN}_{xs} = \frac{\displaystyle\int_{D_{xw}}^{\infty} D_x^{\alpha_x} e^{-\lambda_x D_x} dD_x \int_0^{\infty} (D_x + D_s)^2 |V_x - V_s| D_s^{\alpha_s} e^{-\lambda_s D_s} dD_s}{\displaystyle\int_0^{\infty} D_x^{\alpha_x} e^{-\lambda_x D_x} dD_x \int_0^{\infty} (D_x + D_s)^2 |V_x - V_s| D_s^{\alpha_s} e^{-\lambda_s D_s} dD_s}. \tag{B.6}$$

b. Collection of cloud droplets and small ice (QXACW, QXACI, NXACI)

The collection of cloud water by other hydrometeor species X ($x = i, r, s, g, h$) is

$$\mathrm{QXACW} = \pi/4 E_{xw} q_w \gamma a_x n_{ox} \Gamma(3 + \alpha_x + b_x) \times (\lambda_x + f_x)^{-(3+\alpha_x+b_x)}, \tag{B.7}$$

where E_{xw} is the mean collection efficiency integrated over all sizes of collector particles and all sizes of cloud droplets. Since accurate calculation of E_{xw} is not possible through analytic means because the collection efficiency $E_{xw}(D_w, D_x)$ is a complex function of the sizes of the droplets and the collector particles (e.g., Hall 1980), E_{xw} is assumed to be unity for each of the hydrometeor categories.

The collection of cloud ice by precipitation ($x = r, s, g, h$) is given by

$$\mathrm{QXACI} = \frac{\pi}{4} E_{xi} q_i \gamma a_x n_{ox} \Gamma(3 + \alpha_x + b_x) \times (\lambda_x + f_x)^{-(3+\alpha_x+b_x)}, \tag{B.8}$$

$$\mathrm{NXACI} = \frac{\pi}{4} E_{xi} n_i \gamma a_x n_{ox} \Gamma(3 + \alpha_x + b_x) \times (\lambda_x + f_x)^{-(3+\alpha_x+b_x)}, \tag{B.9}$$

where E_{xi} represents the collection efficiency of ice crystals by precipitation particles larger than D_{xi} (40 μm) in diameter. The collection efficiencies of small crystals by rain, snow, and rimed ice (graupel and frozen drops/hail), respectively, are

$$E_{ri} = 1 - \gamma^*[3 + \alpha_r + b_r, (\lambda_r + f_r)D_{ri}], \tag{B.10}$$

$$E_{si} = E_{si1} \exp(E_{si2} T_c)\{1 - \gamma^*[3 + \alpha_s + b_s, \lambda_s D_{si}]\}, \tag{B.11}$$

$$E_{xy} = E_{xy1} \exp(E_{xy2} T_c)[\gamma^*(3 + \alpha_x + b_x, \lambda_x D_{xw}) - \gamma^*(3 + \alpha_x + b_x, \lambda_x D_{xi})] + (E_{xy})_{\mathrm{wet}} \times [1 - \gamma^*(3 + \alpha_x + b_x, \lambda_x D_{xw})], \tag{B.12}$$

where $E_{si1} = 0.25$ and $E_{si2} = 0.05$ in (B.11) were estimated from Kajikawa and Heymsfield (1989), $E_{xy1} = E_{xy2} = 0.1$ in (B.12) describe the collection efficiencies of ice crystals and snow by dry graupel and dry frozen drops/hail ($x = g, h$; $y = i, s$), and $(E_{xy})_{\mathrm{wet}} = 1$ is assumed for the collection of cloud ice and snow by wet, rimed precipitation ice.

As more detailed laboratory results become available, accurate calculations of the integrated collection efficiencies (E_{xw}, E_{xi}) can be incorporated into the parameterization by storing their numerical solutions in lookup tables as functions of the mean droplet diameter (D_w) and the slope (λ_x) of the particle spectra.

c. Diameters D_{1xy}, D_{2xy} in riming conversion (QXACWX, QXACWY, QWACXY, NWACXY)

Particle diameters D_{1sg}, D_{1gh}, and D_{1hg} [symbolized by D_{1xy} in Eqs. (4.27)–(4.30)] are the minimum particle sizes in which the density of the accreted rime is equal to ρ_g (conversion from snow to graupel), ρ_h (conversion from graupel to frozen drops), and ρ_g(conversion from frozen drops to graupel), respectively. A minimum diameter threshold of 0.05 cm is typically assumed for D_{1xy}. Rime densities were calculated using Heymsfield and Pflaum (1985) and the detailed parameterization of impact velocities by Rasmussen and Heymsfield (1985). Values of D_{1xy} were solved by numerical iteration, and the solutions stored in three-dimensional lookup tables at discrete values of mean droplet diameter (D_w), cloud temperature (T_c in °C), and height [variation of γ with height; see Eq. (3.7)]. Table A1 shows the organization of the lookup tables for D_{1sg}, D_{1gh}, and D_{1hg}. These tables need to be created only when using a different input environment or when the vertical resolution in the model is modified (the GCE model allows for variable stretched vertical coordinates).

Particle diameter D_{2xy} represents the size in which the particle mass (m_x) doubles within time interval $\Delta t_{\rm rime}$, and it is solved by using the following collection equation,

$$dm_x/dt = \pi/4 E_{xw}\gamma\rho q_w a_x D_x^{2+b_x}, \qquad \text{(B.13)}$$

and by assuming that the density of the accreted rime is that of the converted particle (ρ_y),

$$dm_x/dt = d(\pi/6\rho_y D_x^3)/dt. \qquad \text{(B.14)}$$

Combining (B.13) and (B.14), integrating over time interval $\Delta t_{\rm rime}$, and representing the final size of the rimed particle by D_{fxy} yields

$$D_{fxy}^{1-b_x} - D_{2xy}^{1-b_x} = \frac{(1-b_x)E_{xw}\rho q_w \gamma a_x (\Delta t)_{\rm rime}}{2\rho_y}. \qquad \text{(B.15)}$$

Since the mass of the particle is assumed to have doubled during $\Delta t_{\rm rime}$,

$$\pi/6\rho_y(D_{fxy}^3 - D_{2xy}^3) = \pi/6\rho_x D_{2xy}^3. \qquad \text{(B.16)}$$

Solving for D_{fxy} in (B.16) and substituting into (B.15), a relationship for D_{2xy} as a function of cloud water content and height (γ) is

$$D_{2xy} = [\tau_{xy}(\Delta t)_{\rm rime}\gamma\rho q_w]^{(1-b_x)^{-1}}, \qquad \text{(B.17)}$$

where

$$\tau_{xy} = \frac{(1-b_x)E_{xw}a_x}{2\rho_y}[(1+\rho_x/\rho_y)^{(1-b_x)/3} - 1]^{-1} \qquad \text{(B.18)}$$

is a constant associated with each riming conversion process (e.g., τ_{sg} is the constant for the processes QSACWG, QWACSG, and NWACSG). Riming conversion occurs only when $D_{1xy} < D_{2xy}$ and $D_{2xy} \geqslant$ 0.02 cm, otherwise QXACWY, QWACXY, and NWACXY are zero and QXACWX is given by (B.7). The minimum cloud droplet diameter for riming conversion, represented by $(D_w)_1$ in Table A1, is obtained by solving for the threshold cloud water content (ρq_w) in (B.17) for $D_{2xy} = 0.02$ cm [i.e., $\rho q_w = \pi/6\rho_L n_w (D_w)_1^3$].

TABLE A1. Data structure of lookup tables for D_{1xy} in (4.27)–(4.30). See discussion after (B.18) for how $(D_w)_1$ is obtained. The factor X_w is scaled such that $(D_w)_{30}$ is the mean cloud droplet diameter for a maximum cloud water content of 5 g m^{-3}.

D_{1sg} (T_c, D_w, z) tables for QSACWS, QSACWG, QWACSG, NWACSG.
- $(T_c)_i = i\Delta T_c$ for $i = 1$ to 40, $\Delta T_c = -0.5$°C (T_c varies from -0.5° to -20°C).
- $(D_w)_i = X_w^{i-1}(D_w)_1$ for $i = 1$ to 30.
- z_i – n vertical levels between 0° and -30°C (typically 7–9 discrete levels, depending upon vertical coordinates used in model).

D_{1gh} (T_c, D_w, z) tables for QGACWG, QGACWH, QWACGH, NWACGH.
- $(T_c)_i = i\Delta T_c$ for $i = 1$ to 40, $\Delta T_c = -0.5$°C (T_c varies from -0.5° to -20°C).
- $(D_w)_i = X_w^{i-1}(D_w)_1$ for $i = 1$ to 30.
- z_i – n vertical levels between 0° and -30°C (typically 7–9 discrete levels, depending upon vertical coordinates used in model).

D_{1hg} (T_c, D_w, z) tables for QHACWH, QHACWG, QWACHG, NWACHG.
- $(T_c)_i = i\Delta T_c - 5$ for $i = 0$ to 35, $\Delta T_c = -1$°C (T_c varies from -5° to -40°C).
- $(D_w)_i = X_w^{i-1}(D_w)_1$ for $i = 1$ to 30.
- z_i – n vertical levels between 0° and -45°C (typically 9–11 discrete levels, depending upon vertical coordinates used in model).

d. Aggregation of small ice and snow (NXACX), breakup of snow (NSBR)

Many studies have recognized the importance of ice aggregation, especially in stratiform clouds (e.g., Lo and Passarelli 1982; Stewart et al. 1984; Churchill and Houze 1984; Gordon and Marwitz 1986; Heymsfield 1986; Houze and Churchill 1987; Willis and Heymsfield 1989; Gamache 1990; Houze et al. 1992). The decrease in the number of concentrations of small ice crystals and snow by aggregation is

$$\mathrm{NXACX} = -\frac{\pi}{8}\gamma a_x n_{ox}^2 \int_0^\infty\int_0^\infty E_{xx}(D_i + D_j)^2 |D_i^{b_x} - D_j^{b_x}| D_j^{\alpha_x} D_i^{\alpha_x} e^{-\lambda_x(D_j+D_i)} dD_j dD_i. \qquad \text{(B.19)}$$

Using an approach similar to Passarelli (1978), the analytic solution to (B.19) is

$$\mathrm{NXACX} = \gamma a_x E_{xx} n_{ox}^2 I(\alpha_x, b_x)\lambda_x^{-(4+2\alpha_x+b_x)}, \qquad \text{(B.20)}$$

$$I(\alpha_x, b_x) = \frac{\pi\Gamma(4+2\alpha_x+b_x)}{2^{6+2\alpha_x+b_x}}\sum_{k=1}^{3} c_k\left[\frac{F^*(k+\alpha_x+1)}{k+\alpha_x} - \frac{F^*(k+\alpha_x+b_x+1)}{k+\alpha_x+b_x}\right], \qquad \text{(B.21)}$$

where $F^*(x) = F(1, 4 + 2\alpha_x + b_x; x; \frac{1}{2})$ is Gauss' hypergeometric function, $c_1 = c_3 = 1$ and $c_2 = 2$, and $I(\alpha_x, b_x)$ is a constant that depends only upon the shape parameter (α_x) and fall speed exponent (b_x) given in Tables 3 and 4, respectively, for small ice and snow. The self-breakup of snow is parameterized implicitly by preventing the slope of the snow distribution from decreasing below a lower limit of λ_{s0}, where aircraft observations and theoretical studies suggest a value of $\lambda_{s0} = 10$ cm^{-1} (Lo and Passarelli 1982; Mitchell 1988).

e. *Freezing rates of liquid water onto precipitation ice (QXFM)*

It was assumed in an earlier version of the model, as well as in other microphysical schemes, that collisional freezing of rain by collection of small ice crystals and snow (QIACR, QSACR) resulted in the complete freezing of the drop. But in simulations where large numbers of ice particles were present, this assumption resulted in the immediate freezing of copious amounts of rain (up to 5 g kg^{-1}) at supercooled air temperatures warmer than -0.5°C. (These situations can occur when active turrets rise in regions where ice particles are already present.) Such rapid glaciation rates are unrealistic and are inconsistent with the time required for the complete freezing of raindrops (Pruppacher and Klett 1978). Since other microphysical parameterizations only limit the freezing rates of liquid water collected on hail during wet growth, the rates of drop freezing by collection of cloud ice and snow in these schemes are also likely to be too rapid (e.g., RH, LFO, COT).

The rate of freezing of liquid water onto a population of precipitation ice ($x = s, g, h$) is

$$\mathrm{QXFM} = \min(\mathrm{XFM1}, \mathrm{XFM2}), \qquad \text{(B.22)}$$

where XFM1 describes the maximum freezing rate of the precipitation ice, which is controlled by the rate that heat is dissipated to the environment by evaporation and conduction, and XFM2 is the amount of liquid water available for freezing. The terms XFM1 and XFM2 are for snow, graupel, and frozen drops/hail, respectively:

$$\mathrm{SFM1} = (1 - \Delta t\mathrm{QWACSG}/q_s)\mathrm{QSFZ}, \qquad \text{(B.23)}$$

$$\begin{aligned}\mathrm{SFM2} = {} & q_{sw}/\Delta t + \mathrm{QSACW} + \mathrm{QSACRS} \\ & - F_{sw}(\mathrm{QWACSG} + \mathrm{QRACSG} + \mathrm{QRACSH} + \mathrm{QGACS} + \mathrm{QHACS}),\end{aligned} \qquad \text{(B.24)}$$

$$\begin{aligned}\mathrm{GFM1} = {} & (1 - \Delta t\mathrm{QWACGH}/q_g)\mathrm{QGFZ} + \Delta t[\mathrm{QRFZ}\cdot\mathrm{QSACRG}/q_r \\ & + \mathrm{QSFZ}\cdot\mathrm{QWACSG}/q_s + \mathrm{QHFZ}\cdot\mathrm{QWACHG}/q_h],\end{aligned} \qquad \text{(B.25)}$$

$$\begin{aligned}\mathrm{GFM2} = {} & q_{gw}/\Delta t + \mathrm{QGACW} + \mathrm{QGACRG} + \mathrm{QSACRG} + \mathrm{QSACWG} \\ & + \mathrm{QHACWG} + F_{gw}(\mathrm{QWACSG} + \mathrm{QRACSG} + \mathrm{QGACS}),\end{aligned} \qquad \text{(B.26)}$$

$$\begin{aligned}\mathrm{HFM1} = {} & (1 - \Delta t\mathrm{QWACHG}/q_h)\mathrm{QHFZ} + \Delta t[(\mathrm{QRFZ}(\mathrm{QIACR} + \mathrm{QSACRH} \\ & + \mathrm{QGACRH})/q_r + \mathrm{QGFZ}\cdot\mathrm{QWACGH}/q_g],\end{aligned} \qquad \text{(B.27)}$$

$$\begin{aligned}\mathrm{HFM2} = {} & q_{hw}/\Delta t + \mathrm{QHACW} + \mathrm{QHACR} + \mathrm{QIACR} + \mathrm{QSACRH} + \mathrm{QGACWH} \\ & + \mathrm{QGACRH} + F_{sw}(\mathrm{QRACSH} + \mathrm{QHACS}) \\ & + F_{gw}(\mathrm{QWACGH} + \mathrm{QRACGH}) - F_{hw}\mathrm{QWACHG}.\end{aligned} \qquad \text{(B.28)}$$

The variables QXFZ ($x = r, s, g, h$) represent the freezing rates derived from the heat balance relationship between the heat gained by freezing and heat lost by evaporation and conduction (Musil 1970; Pruppacher and Klett 1978):

$$\mathrm{QRFZ} = \min[q_r/\Delta t, \max(0, X_1 n_{or}\cdot \mathrm{VENT}_r)], \qquad \text{(B.29)}$$

$$\mathrm{QSFZ} = \max(0, X_1\cdot n_{os}\cdot \mathrm{VENT}_s + X_2\cdot \mathrm{QSACI}), \qquad \text{(B.30)}$$

$$\begin{aligned}\mathrm{QGFZ} = {} & \max[0, X_1\cdot n_{og}\cdot \mathrm{VENT}_g \\ & + X_2\cdot(\mathrm{QGACI} + \mathrm{QGACS})],\end{aligned} \qquad \text{(B.31)}$$

$$\begin{aligned}\mathrm{QHFZ} = {} & \max[0, X_1\cdot n_{oh}\cdot \mathrm{VENT}_h \\ & + X_2\cdot(\mathrm{QHACI} + \mathrm{QHACS})],\end{aligned} \qquad \text{(B.32)}$$

where X_1 and X_2 are defined as

$$X_1 = X_3/(1 + c_w T_c/L_f), \qquad \text{(B.33)}$$

$$X_2 = -C_i T_c/(L_f + c_w \Delta T_c), \qquad \text{(B.34)}$$

$$X_3 = 2\pi/L_f\{L_s\psi[q_{ws}(0°\text{C}) - q_v] - \rho^{-1}K_aT_c\}, \quad (\text{B.35})$$

ψ is the diffusivity of water vapor in air, K_a is the thermal conductivity of air,

$$\text{VENT}_x = A_x \frac{\Gamma(2+\alpha_x)}{\lambda_x^{2+\alpha_x}} + B_x S_c^{1/3}\left(\frac{\gamma a_x}{\nu}\right)^{1/2} \times \frac{\Gamma(2.5+\alpha_x+0.5b_x)}{(\lambda_x+f_x)^{2.5+\alpha_x+0.5b_x}} \quad (\text{B.36})$$

is the ventilation effects associated with falling precipitation integrated over the particle size distributions using (3.2) and (3.7), ν is the kinematic viscosity, Sc ($=\nu/\psi$) is the Schmidt number, and $A_x = 0.78$ and $B_x = 0.31$ are the ventilation coefficients assumed for precipitation (Beard and Pruppacher 1971).

Melting of precipitation is treated in a manner similar to other schemes, where

$$\text{QXFM} = \min[0, X_4 n_{ox}\cdot\text{VENT}_x - c_w T_c(\text{QXACW} + \text{QXACR})/L_f]. \quad (\text{B.37})$$

In order to prevent unrealistic temperature oscillations across the 0°C, the combined freezing and melting rates, respectively, of all hydrometeors were limited near 0°C as follows:

$$\text{QSFM} + \text{QGFM} + \text{QHFM} \leqslant -0.5C_p\Delta T_{\text{frz}}/L_f, \quad (\text{B.38})$$

$$\Delta T_{\text{frz}} = T_c + \Delta t L_f/C_p(\text{QIFM} + \text{QIACW} + \text{QIHR}) + \Delta t L_v/C_p(\text{QCND} + \text{QREVP}) + \Delta t L_s/C_p(\text{QINT} + \text{QIDEP} + \text{QSDEP} + \text{QGDEP} + \text{QHDEP}), \quad (\text{B.39})$$

$$\text{QSFM} + \text{QGFM} + \text{QHFM} \geqslant -0.5C_p\Delta T_{mlt}/L_f, \quad (\text{B.40})$$

$$\Delta T_{mlt} = T_c + \Delta t L_v/C_p(\text{QCND} + \text{QREVP} + \text{QSEVP} + \text{QGEVP} + \text{QHEVP}) + \Delta t L_f \text{QIFM}/C_p, \quad (\text{B.41})$$

causing gridpoint temperatures near the freezing level to oscillate above and below 0°C at subsequent time steps.

f. Shedding of liquid water (QXSHD, NXSHD)

The rates that liquid water is shed due to the complete melting of ice at $T_c > 0$°C are

$$\text{QSSHD} = \max(0, q_s/\Delta t + \text{QSACW} + \text{QSACR} + \text{QSEVP} - \text{QGACS} - \text{QHACS}), \quad (\text{B.42})$$

$$\text{QGSHD} = \max(0, q_g/\Delta t + \text{QGACW} + \text{QGACR} + \text{QGEVP} + \text{QGACS}), \quad (\text{B.43})$$

$$\text{QHSHD} = \max(0, q_h/\Delta t + \text{QHACW} + \text{QHACR} + \text{QHEVP} + \text{QHACS}). \quad (\text{B.44})$$

Otherwise, the rates in which excess amounts of liquid water are shed from large ice (at all temperatures) are

$$\text{QXSHD} = \max[0, q_{xw} - F_{wm}(q_x^* - q_{xw}^*) \div (1 - F_{wm})]/\Delta t, \quad (\text{B.45})$$

where q_x^* and q_{xw}^* are dummy values at time $t + \Delta t$ calculated as a result of all of the other microphysical processes, such that

$$q_x^* = q_x + \Delta t(dq_x/dt + \text{QXSHD}), \quad (\text{B.46})$$

$$q_{xw}^* = q_{xw} + \Delta t(dq_{xw}/dt + \text{QXSHD}), \quad (\text{B.47})$$

and dq_x/dt and dq_{xw}/dt are given by (A.5)–(A.7) and (A.8)–(A.10), respectively.

The number concentrations of precipitation ice change when liquid water is shed during melting by assuming that the slopes of the particle distributions are approximately constant:

$$\text{NSSHD} = (n_s/q_s)\max(0, \text{QSSHD} - \text{QSACW} - \text{QSACR}), \quad (\text{B.48})$$

$$\text{NGSHD} = (n_g/q_g)\max(0, \text{QGSHD} - \text{QGACW} - \text{QGACR} - \text{QGACS}), \quad (\text{B.49})$$

$$\text{NHSHD} = (n_h/q_h)\max(0, \text{QHSHD} - \text{QHACW} - \text{QHACR} - \text{QHACS}). \quad (\text{B.50})$$

g. Evaporation and deposition onto precipitation (QXEVP, NXEVP, QXDEP, NXDEP)

Evaporation from rain and condensation (or evaporation) from melting precipitation ice (x = s, g, h) are, respectively,

$$\text{QREVP} = 2\pi \text{SS}_w n_{or}\text{VENT}_r/\text{AB}_w, \quad (\text{B.51})$$

$$\text{QXEVP} = 2\pi\psi[\text{qv} - \text{qws}(0°\text{C})]\text{n}_{ox}\text{VENT}_x, \quad (\text{B.52})$$

where VENT_x is given by (B.36) for rain and precipitation ice, $\text{SS}_w = q_v/q_{ws} - 1$ is the subsaturation ratio with respect to water, and

$$\text{AB}_w = \frac{L_v^2}{K_aR_vT^2} + \frac{1}{\rho q_{ws}\psi}, \quad (\text{B.53})$$

The rates of depositional growth or decay of precipitation ice are

$$\text{QXDEP} = 2\pi\text{SS}_i n_{ox}\text{VENT}_x/\text{AB}_i, \quad (\text{B.54})$$

where SS_i is the subsaturation ratio with respect to ice, and

$$\text{AB}_i = \frac{L_s^2}{K_aR_vT^2} + \frac{1}{\rho q_{is}\psi},$$

The rates in which the number concentrations of precipitation ice are reduced by sublimation (QXDEP

< 0) of dry ice and evaporation of wet ice (QXEVP < 0), respectively, are

$$\mathrm{NXDEP} = (n_x/q_x)\cdot\mathrm{QXDEP}, \quad (B.55)$$

$$\mathrm{NXEVP} = (n_x/q_x)\cdot\mathrm{QXEVP}, \quad (B.56)$$

where λ_x of the particle distributions are assumed to be constant as in (B.48)–(B.50).

h. Autoconversion of cloud water to rain (QRAUT)

Autoconversion of cloud water to rain (QRAUT) commences when the mean drop diameter reaches a value of $D_{wa} = 20\ \mu$m, such that autoconversion is delayed in continental environments with large droplet number concentrations (Manton and Cotton 1977; Cotton et al. 1982; Banta and Hanson 1987). The Orville and Kopp (1977) modification of Berry's (1968) formula is used for the autoconversion of cloud water to rain,

$$\mathrm{QRAUT} = \rho(q_w - q_{w0})/[1.2\times10^{-4} + 1.596 \times 10^{-12} n_w/\phi\rho(q_w - q_{w0})], \quad (B.57)$$

except that the threshold cloud water mixing ratio for autoconversion is allowed to vary with droplet concentration as

$$q_{w0} = \rho^{-1}\pi/6\rho_L n_w D_{wa}^3. \quad (B.58)$$

i. Cloud water condensation and cloud ice deposition (QCND, QIDEP, NIDEP)

Condensation of cloud water is calculated using the saturation technique of Soong and Ogura (1973),

$$\mathrm{QCND} = \max\left\{-\frac{q_c}{\Delta_t}, \frac{q_v - q_{ws}}{\Delta t\left[1 + \dfrac{4098.026L_v q_{ws}}{C_p(T - 35.86)^2}\right]}\right\}, \quad (B.59)$$

where q_v and q_{ws} are the dummy values of the actual water vapor mixing ratio and the water vapor mixing at water saturation, respectively, calculated at time $t + \Delta t$ as a result of advection and diffusion. The saturation water vapor mixing ratio is calculated using Teten's formula. This method does not allow model grid points to be supersaturated with respect to water.

Deposition onto small ice crystals is calculated using an approach similar to (B.54),

$$\mathrm{QIDEP} = 2\pi \mathrm{SS}_i n_{oi}\mathrm{VENT}_i/\mathrm{AB}_i. \quad (B.60)$$

However, the expression representing the ventilation effects of small ice crystals (VENT_i) is more complicated than for precipitation [VENT_x is given by Eq. (B.36)]. The ventilation effect of small ice integrated over all particle sizes is

$$\mathrm{VENT}_i = \int_0^\infty \mathrm{VF}_i(D_i)D_i^{1+\alpha_i}e^{-\lambda_i D_i}dD_i, \quad (B.61)$$

where

$$\mathrm{VF}_i(D_i) = \begin{cases} 1 + 0.14\chi_i^2, & \chi_i < 1.0 \\ 0.86 + 0.28\chi_i, & \chi_i \geq 1.0 \end{cases} \quad (B.62)$$

is the ventilation coefficients of ice crystals taken from Hall and Pruppacher (1976) with $\chi_i(D_i) = \mathrm{Sc}^{1/3}\,\mathrm{Re}^{1/2}$ and $\mathrm{Re} = V_i D_i/\nu$. Substituting (B.62) into (B.61) yields

$$\begin{aligned}\mathrm{VENT}_i = {} & \frac{\Gamma(2+\alpha_i)}{\lambda_i^{2+\alpha_i}} \\ & \times [0.86 + 0.14\gamma^*(2+\alpha_i, \lambda_i D_{if})] \\ & + 0.14\varphi_i^2\frac{\Gamma(3+\alpha_i+b_i)}{\lambda_i^{3+\alpha_i+b_i}} \\ & \times \gamma^*(3+\alpha_i+b_i, \lambda_i D_{if}) \\ & + 0.28\varphi_i\frac{\Gamma(2.5+\alpha_i+0.5b_i)}{\lambda_i^{2.5+\alpha_i+0.5b_i}} \\ & \times [1 - \gamma^*(2.5+\alpha_i+0.5b_i, \lambda_i D_{if})],\end{aligned} \quad (B.63)$$

where D_{if} is defined as the size of an ice crystal such that $\chi_i(D_{if}) = 1$, and $\varphi_i = (\gamma a_i)^{1/2}(\nu^{1/2}\psi)^{-1/3}$. Reductions in the number concentrations of small ice crystals by sublimation (NIDEP < 0) are calculated in a similar manner as for precipitation ice in (B.55) by assuming λ_i is approximately constant during sublimation.

j. Rime-splintering mechanisms (QIHMX, NIHMX)

Based upon the laboratory experiments of Mossop (1985), and using (3.2) and (3.7), the rate at which ice splinters are produced by riming onto precipitation ice is

$$\mathrm{NIHMX} = \pi/4\gamma a_x n_{ox}\mathrm{HM}_T\mathrm{HM}_w \times \int_0^\infty E_{xw}\mathrm{HM}_x D_x^{2+\alpha_x+b_x}e^{-\lambda_x D_x}dD_x, \quad (B.64)$$

where the quantitative effects of temperature, droplet sizes, and rime fall velocities upon ice splinter production are represented by the functional relationships HM_T, HM_w, and HM_x, respectively. It is assumed in (B.64) that $f_x = 0$ for precipitation ice.

For temperatures between −2° and −8°C, the dependence of temperature upon crystal production is

$$\mathrm{HM}_T = \begin{cases} 0.5, & -2^\circ \leq T_c < -4^\circ\mathrm{C} \\ 1.0, & -4^\circ \leq T_c \leq -6^\circ\mathrm{C} \\ 0.5, & -6^\circ < T_c \leq -8^\circ\mathrm{C} \\ 0, & \text{otherwise.} \end{cases} \quad (B.65)$$

This functional relationship using air temperature rather than the surface temperature of the particle, as suggested by Heymsfield and Mossop (1984), is based upon an approximate representation of Fig. 3 in Mossop (1985), as well as taking into account the limited vertical resolution with respect to temperature in all cloud models.

The number of splinters was found by Mossop to vary as a function of the number of large drops rimed onto the falling ice particle, such that

$$\mathrm{HM}_w = n_{wl}^*[10^{-2} + 1.5\cdot 10^{-3}\log(n_{ws}^*/n_{wl}^*)], \quad \text{(B.66)}$$

in which n_{ws}^* and n_{wl}^* are the number concentrations of small ($\leq 12\ \mu$m) and large ($\geq 25\ \mu$m) droplets, respectively, that are rimed onto the precipitation ice particle. Since Mossop (1985) found that

$$n_{ws}^*/n_{wl}^* \sim 1/3(n_{ws}/n_{wl}), \quad \text{(B.67)}$$

where n_{ws} and n_{wl} are the number concentrations of small ($\leq 12\ \mu$m) and large ($\geq 25\ \mu$m) droplets, respectively, then substituting (B.67) into (B.66) and assuming that $n_{wl}^* \sim n_{wl}$ yields

$$\mathrm{HM}_w = n_{wl}[9.3\cdot 10^{-3} + 1.5\cdot 10^{-3}\log(n_{ws}/n_{wl})]. \quad \text{(B.68)}$$

Expressions for n_{ws} and n_{wl} are then obtained by integrating (3.1) over the appropriate range of droplet sizes:

$$n_{ws} = n_w\left\{1 - \exp\left[-\frac{\pi\rho_L n_w(12\times 10^{-4})^3}{6\rho q_w}\right]\right\}, \quad \text{(B.69)}$$

$$n_{wl} = n_w \exp\left[-\frac{\pi\rho_L n_w(25\times 10^{-4})^3}{6\rho q_w}\right]. \quad \text{(B.70)}$$

The effect of rime fall velocity upon crystal production is parameterized based on Fig. 4a of Mossop (1985) as

$$\mathrm{HM}_x = \begin{cases} V_x/200, & 0 < V_x\ (\mathrm{cm\ s^{-1}}) < 200 \\ 1, & 200 \leq V_x \leq 400 \\ (600 - V_x)/200, & 400 < V_x \leq 600. \end{cases} \quad \text{(B.71)}$$

Substituting (B.71) into (B.64), assuming $E_{xw} = 1$, and rearranging terms produces

$$\mathrm{NIHMX} = (\pi/4)\gamma a_x n_{ox}\cdot\mathrm{HM}_T\cdot\mathrm{HM}_w\cdot\mathrm{HMV}_x, \quad \text{(B.72)}$$

$$\mathrm{HMV}_x = \frac{\gamma a_x}{200}\left[\int_0^{D_{\mathrm{HM1}}} D_x^{2(1+b_x)+\alpha_x}e^{-\lambda_x D_x}dD_x - \int_{D_{\mathrm{HM2}}}^{D_{\mathrm{HM3}}} D_x^{2(1+b_x)+\alpha_x}e^{-\lambda_x D_x}dD_x\right] + \int_{D_{\mathrm{HM1}}}^{D_{\mathrm{HM2}}} D_x^{2+b_x+\alpha_x}e^{-\lambda_x D_x}dD_x + 3\int_{D_{\mathrm{HM2}}}^{D_{\mathrm{HM3}}} D_x^{2+b_x+\alpha_x}e^{-\lambda_x D_x}dD_x, \quad \text{(B.73)}$$

in which the range of ice particle diameters are defined by $\gamma a_x D_{\mathrm{HM1}}^{b_x} = 200$ cm s^{-1}, $\gamma a_x D_{\mathrm{HM2}}^{b_x} = 400$ cm s^{-1}, and $\gamma a_x D_{\mathrm{HM3}}^{b_x} = 600$ cm s^{-1}. Integrating each of the terms in (B.73) and using the modified gamma probability function gives

$$\mathrm{HMV}_x = \Gamma(3 + 2b_x + \alpha_x)\gamma a_x \lambda_x^{-(3+2b_x+\alpha_x)}\frac{\mathrm{HM}_{x1}}{200} + \Gamma(3 + b_x + \alpha_x)\lambda_x^{-(3+b_x+\alpha_x)}\mathrm{HM}_{x2}, \quad \text{(B.74)}$$

where

$$\mathrm{HM}_{x1} = \gamma^*[3 + 2b_x + \alpha_x, \lambda_x(200/\gamma a_x)^{1/b_x}] + \gamma^*[3 + 2b_x + \alpha_x, \lambda_x(400/\gamma a_x)^{1/b_x}] - \gamma^*[3 + 2b_x + \alpha_x, \lambda_x(600/\gamma a_x)^{1/b_x}], \quad \text{(B.75)}$$

$$\mathrm{HM}_{x2} = 3\gamma^*[3 + b_x + \alpha_x, \lambda_x(600/\gamma a_x)^{1/b_x}] - \gamma^*[3 + 2b_x + \alpha_x, \lambda_x(200/\gamma a_x)^{1/b_x}] - 2\gamma^*[3 + 2b_x + \alpha_x, \lambda_x(400/\gamma a_x)^{1/b_x}]. \quad \text{(B.76)}$$

Assuming a characteristic diameter for the ice splinters (D_{im}) of 0.01 cm, the mass generation of small ice crystals by cloud water riming onto snow, graupel, and hail/frozen drops ($x = s, g, h$) is

$$\mathrm{QIHMX} = \rho^{-1}c_i(D_{im})^{d_i}\mathrm{NIHMX}, \quad \text{(B.77)}$$

where NIHMX is given by substituting (B.65), (B.68)–(B.70), and (B.74)–(B.76) into (B.72).

k. *Ice enhancement (QIHR, NIHR)*

The observations summarized in Hobbs (1990) are the basis for this parameterization, such that

$$n_{i\max}(L^{-1}) = (D_t/16\ \mu\mathrm{m})^7 \quad \text{(B.78)}$$

is the maximum ice particle number concentration, and D_t is a threshold droplet diameter where the number concentration of all droplets larger than D_t is 3 cm^{-3}. Defining the threshold droplet volume $v_t = \pi/6D_t^3$, integrating over all droplet volumes larger than v_t using (3.1), and substituting into (B.78), an expression for the maximum ice crystal number concentration is

$$n_{i\max}(\mathrm{cm^{-3}}) = 1.69\cdot 10^{17}\left[\frac{\ln(n_w/3)}{n_w}\right]^{7/3}(\rho q_w)^{7/3}. \quad \text{(B.79)}$$

Differentiating (B.79) with respect to time and making the simple assumption that NIHR and $n_{i\max}/\Delta t_{\mathrm{HR}}$ with values of $\Delta t_{\mathrm{HR}} = 300$ s, then the rate of the Hobbs–Rangno ice enhancement mechanism becomes

$$\mathrm{NIHR} = \frac{1.69\cdot 10^{17}}{\Delta t_{\mathrm{HR}}}\left[\frac{\rho q_w}{n_w}\ln\left(\frac{n_w}{3}\right)\right]^{7/3}, \quad \text{(B.80)}$$

$$\mathrm{QIHR} = \rho^{-1}c_i(D_{i\mathrm{HR}})^{d_i}\mathrm{NIHR}, \quad \text{(B.81)}$$

and $D_{i\mathrm{HR}}$ is assumed to be 0.01 cm.

APPENDIX C

Radar Reflectivity Calculations

The total equivalent radar reflectivity factor (Z_{et} in $mm^6\ m^{-3}$) is calculated from the sum of the reflectivities for all hydrometeor species,

$$Z_{et} = Z_{er} + Z_{ei} + Z_{es} + Z_{eg} + Z_{eh}, \quad (C.1)$$

where the reflectivity for each hydrometeor category ($x = r, i, s, g, h$) using (3.2) is

$$Z_{ex} = 10^{12} n_{ox} \int_0^\infty \frac{|K|_x^2}{|K|_w^2} D_x^{6+\alpha_x} e^{-\lambda_x D_x} dD_x, \quad (C.2)$$

and $|K|_x^2$ and $|K|_w^2$ are $|K|^2$ for ice species X and liquid water, respectively.

The equivalent radar reflectivity for raindrops is

$$Z_{er} = 10^{12}\Gamma(7 + \alpha_r) n_{or} \lambda_r^{-(7+\alpha_r)} \quad (C.3)$$

with $|K|_r^2 = |K|_w^2$ in (C.2), and n_{or} and λ_r are defined in section 3a for either exponential or gamma drop size distributions.

For dry ice particles ($x = i, s, g, h$) the radar reflectivity factor is

$$Z_{ex} = 10^{12} n_{oxm} \int_0^\infty \frac{|K|_i^2}{|K|_w^2} D_{xm}^{6+\alpha_x} e^{-\lambda_{xm} D_{xm}} dD_{xm}, \quad (C.4)$$

where D_{xm} is the melted diameter of the particles, n_{oxm} and λ_{xm} are the parameters for the melted equivalent ice distributions, and $|K|_i^2/|K|_w^2 = 0.224$ (Smith 1984). Integrating (C.4) over all particle sizes yields

$$Z_{ex} = 0.224 \times 10^{12}\Gamma(7 + \alpha_x) n_{oxm} \lambda_{xm}^{-(7+\alpha_x)}. \quad (C.5)$$

The number concentration and mass content for a melted ice particle distribution, respectively, are

$$n_x = \Gamma(1 + \alpha_x) n_{oxm} \lambda_{xm}^{-(1+\alpha_x)}, \quad (C.6)$$

$$Rq_x = \pi/6\rho_L \Gamma(4 + \alpha_x) n_{oxm} \lambda_{xm}^{-(4+\alpha_x)}. \quad (C.7)$$

Combining (C.5)–(C.7) yields a general expression for the radar reflectivity of dry ice particles as a function of their mass and number concentrations:

$$Z_{ex} = C_x'(\rho q_x)^2/n_x, \quad (C.8)$$

$$C_x' = 0.224 \times 10^{12}(6/\pi\rho_L)^2\Gamma(7 + \alpha_x) \times \Gamma(1 + \alpha_x)/\Gamma(4 + \alpha_x)^2, \quad (C.9)$$

where $C_x' = 1.63410^{13}$ for exponential ice distributions ($\alpha_x = 0$ for $x = i, s, g, h$).

For simplicity the dielectric factor of wet precipitation ice ($x = s, g, h$) is calculated from the mass-weighted dielectric factors of water and ice using the theory of Debye (Battan 1973), such that

$$|K|^2 = [|K|_i^2(q_x - q_{xw}) + |K|_w^2 q_{xw}]/q_x. \quad (C.10)$$

Substituting (C.10) into (C.4) and proceeding in the same manner as in the previous paragraph, the radar backscatter from wet precipitation ice is calculated as

$$Z_{ex} = C_x\rho^2(0.224q_x + 0.776q_{xw})q_x/n_x, \quad (C.11)$$

$$C_x = 10^{12}(6/\pi\rho_L)^2\Gamma(7 + \alpha_x)\Gamma(1 + \alpha_x)/\Gamma(4 + \alpha_x)^2, \quad (C.12)$$

in which $C_x = 7.295 \times 10^{13}$ for $\alpha_x = 0$. Equation (C.11) is a general radar relationship that is used for both dry and wet ice particles, since it is equivalent to (C.8) when $q_{xw} = 0$.

APPENDIX D

Derivation of R_Z in (6.5)–(6.6)

The factor R_Z conserves the D^6 moment (i.e., radar reflectivity) when converting from gamma ($\alpha_r \neq 0$) to exponential drop size distributions. The number concentrations (n_r), mass contents (ρq_r), and radar reflectivities (Z_r) for rain distributions given by (3.3) are, respectively:

$$n_r = \Gamma(1 + \alpha_r) n_{or} \lambda_r^{-(1+\alpha_r)}, \quad (D.1)$$

$$rq_r = \pi/6\rho_L \Gamma(4 + \alpha_r) n_{or} \lambda_r^{-(4+\alpha_r)}, \quad (D.2)$$

$$Z_r = 10^{12}\Gamma(7 + \alpha_r) n_{or} \lambda_r^{-(7+\alpha_r)}. \quad (D.3)$$

Substitution of (D.1) into (D.2) and (D.3) and noting that $\rho_L = 1$ yields

$$\rho q_r = (\pi/6)[\Gamma(4 + \alpha_r)/\Gamma(1 + \alpha_r)] n_r \lambda_r^{-3}, \quad (D.4)$$

$$Z_r = 10^{12}[\Gamma(7 + \alpha_r)/\Gamma(1 + \alpha_r)] n_r \lambda_r^{-6}. \quad (D.5)$$

A general expression for Z_r as a function of ρq_r and n_r is then obtained by solving for λ_r^{-3} in (D.4) and incorporating the result in (D.5),

$$Z_r = (6/\pi)^2 10^{12}[\Gamma(7 + \alpha_r)\Gamma(1 + \alpha_r)/\Gamma(4 + \alpha_r)^2] \times (\rho q_r)^2/n_r. \quad (D.6)$$

Changing the shape parameter of the drop size distribution from α_r to α_{rx} produces a reflectivity, mass content, and number concentration of the new raindrop spectrum of Z_{rx}, ρq_{rx}, and n_{rx}, respectively. By equating the reflectivity and mass contents of the raindrop spectra (i.e., $Z_r = Z_{rx}$ and $q_r = q_{rx}$), then $n_{rx} = R_Z n_r$ with

$$R_z = \frac{\Gamma(7 + \alpha_{rx})\Gamma(1 + \alpha_{rx})[\Gamma(4 + \alpha_r)]^2}{\Gamma(7 + \alpha_r)\Gamma(1 + \alpha_r)[\Gamma(4 + \alpha_{rx})]^2}. \quad (D.8)$$

For $\alpha_r = 2.5$ and $\alpha_{rx} = 0$ (as assumed for ice) $R_Z = 4.181$. When n_r is used instead of $R_Z n_r$ in (6.5) and (6.6), the radar reflectivity will increase artificially by 6.2 dB ($Z_{rx}/Z_r = R_Z = 4.181$) as a result of conserving number concentration when $a_r = 2.5$ drop distributions are converted into $\alpha_{rx} = 0$ drop size spectra.

APPENDIX E

List of Symbols Not Referenced in Tables 1 and 2

Symbol	Description	Value	Units
a_2	Constant for ice saturation mixing ratio	5807.7	K
a_g	Fall speed constant for graupel	351.2	$cm^{(1-b_g)}\ s^{-1}$
a_h	Fall speed constant for frozen drops/hail	1094.3	$cm^{(1-b_h)}\ s^{-1}$
a_i	Fall speed constant for ice crystals		$cm^{(1-b_i)}\ s^{-1}$
a_r	Fall speed constant for raindrops	4854	$cm^{(1-b_r)}\ s^{-1}$
a_s	Fall speed constant for snow		$cm^{(1-b_s)}\ s^{-1}$
a_x	Fall speed constant for an particle species x		$cm^{(1-b_x)}\ s^{-1}$
a_z	Fall speed constant for an particle species z		$cm^{(1-b_z)}\ s^{-1}$
A'	Exponent in Bigg freezing of cloud droplets	−.66	K^{-1}
AB_i	Thermodynamic term in deposition onto ice		$cm^2\ s^{-1}$
AB_w	Thermodynamic term in evaporation of rain and wet precipitation ice		$cm^2\ s^{-1}$
A_x	First constant for ventilation of precipitation	.31	
b_g	First fall speed exponent for graupel	.37	
b_h	First fall speed exponent for frozen drops/hail	.6384	
b_i	First fall speed exponent for ice crystals		
b_r	First fall speed exponent for raindrops	1	
b_s	First fall speed exponent for snow		
b_x	First fall speed exponent for species x		
b_z	First fall speed exponent for species z		
B'	Constant in Bigg freezing of cloud droplets	10^{-4}	$cm^{-3}\ s^{-1}$
B_x	Second constant for ventilation of precipitation	.78	
c_g	Mass constant for graupel	$\pi/6\rho_g$	$g\ cm^{-3}$
c_h	Mass constant for frozen drops/hail	$\pi/6\rho_h$	$g\ cm^{-3}$
c_i	Mass constant for ice crystals	.044	$g\ cm^{-3}$
c_r	Mass constant for raindrops	$\pi/6$	$g\ cm^{-3}$
c_s	Mass constant for snow	$\pi/6\rho_s$	$g\ cm^{-3}$
c_x	Mass constant for a species x		$g\ cm^{-d_x}$
c_w	Specific heat of water	4187	$J\ kg^{-1}\ K^{-1}$
c_z	Mass exponent for a species z		$g\ cm^{-d_z}$
C_p	Specific heat of air at constant pressure	1005	$J\ kg^{-1}\ K^{-1}$
C_x	Constant in radar reflectivity of wet ice species x		
C'_x	Constant in radar reflectivity of dry ice species x		
CND	Change in water vapor mixing ratio by net condensation		$g\ g^{-1}$
d_g	Mass exponent for graupel	3	
d_h	Mass exponent for frozen drops/hail	3	
d_i	Mass exponent for ice crystals	3	
d_r	Mass exponent for raindrops	3	
d_s	Mass exponent for snow	3	
d_x	Mass exponent for a species x		
d_z	Mass exponent for a species z		
D_1	Lower threshold diameter in rain collection (QXACRY, QRACXY)		cm
D_{1gh}	Minimum diameter of graupel converted by riming to frozen drops/hail		cm
D_{1hg}	Minimum diameter of frozen drops/hail converted by riming to graupel		cm
D_{1sg}	Minimum diameter of snow converted by riming to graupel		cm
D_{1xy}	Minimum diameter of species x converted to species y by riming		cm
D_2	Larger threshold diameter in rain collection (QXACRY, QRACXY)		cm
D_{2xy}	Maximum diameter of species x converted to species y by riming		cm

APPENDIX E—Continued

Symbol	Description	Value	Units
D_{fxy}	Final diameter of species x that is converted by riming to species y		cm
D_g	Graupel particle diameter		cm
D_h	Frozen drop/hail particle diameter		cm
D_i	Ice crystal diameter		cm
D_{if}	Ice crystal diameter where $x_i = 1$		cm
$D_{i\mathrm{HR}}$	Diameter of ice crystals initiated by ice enhancement	.01	cm
D_{im}	Diameter of ice splinters	.01	cm
$D_{i\max}$	Maximum size of ice crystals, converted to snow	.05	cm
D_{0r}	Median raindrop diameter		cm
D_r	Raindrop diameter		cm
D_{ri}	Minimum diameter of drops collecting cloud ice	40	μm
D_s	Snow particle diameter		cm
D_{si}	Minimum diameter of snow collecting cloud ice	40	μm
D_t	Threshold cloud droplet diameter for ice enhancement		cm
D_w	Cloud droplet diameter		cm
D_{wa}	Mean cloud droplet diameter for autoconversion	20	μm
$D_{w\min}$	Minimum mean cloud droplet diameter	5	μm
D_x	Diameter of particle species x		cm
D_{x1}, D_{x2}	Diameters of colliding ice crystals and snowflakes of different sizes in aggregation process		cm
D_{xi}	Minimum diameter that graupel and frozen drops collect cloud ice	40	μm
D_{xm}	Equivalent melted diameter for ice species x		cm
D_{xw}	Minimum diameter that an ice particle of species x becomes wet		cm
D_z	Diameter of particle species z		cm
DEP	Change in water vapor mixing ratio due to net deposition		g g^{-1}
E_{ri}	Efficiency of rain collecting ice crystals		
E_{si1}	Constant for efficiency of dry snow collecting ice crystals	.25	
E_{si2}	Exponent for efficiency of dry snow collecting ice crystals	.05	K^{-1}
E_{xi}	Efficiency of species x collecting ice crystals		
E_{xr}	Efficiency of species x collecting rain		
$(E_{xs})_{\mathrm{dry}}$	Efficiency of snow collected by dry graupel, frozen drops		
$(E_{xs})_{\mathrm{wet}}$	Efficiency of snow collected by wet graupel, frozen drops	1	
E_{xw}	Efficiency of species x collecting cloud droplets	1	
E_{xx}	Aggregation efficiencies of ice crystals and snow		
E_{xy1}	Constant for efficiency of dry graupel and frozen drops collecting ice crystals and snow	.1	
E_{xy2}	Exponent for efficiency of dry graupel and frozen drops collecting ice crystals and snow	.1	K^{-1}
$(E_{xy})_{\mathrm{wet}}$	Efficiency of wet graupel and frozen drops collecting ice crystals and snow	1	
E_{xz}	Efficiency of species x collecting species z		
f_g	Second fall speed exponent for graupel	0	cm^{-1}
f_h	Second fall speed exponent for frozen drops/hail	0	cm^{-1}
f_i	Second fall speed exponent for ice crystals	0	cm^{-1}
f_r	Second fall speed exponent for raindrops	1.95	cm^{-1}
f_s	Second fall speed exponent for snow	0	cm^{-1}
f_x	Second fall speed exponent for species x		
f_z	Second fall speed exponent for species z		
F^*	Notation for Gauss' hypergeometric function		
F_{gw}	Liquid water mass fraction on graupel		
F_{hw}	Liquid water mass fraction on frozen drops/hail		
F_{sw}	Liquid water mass fraction on snow		

APPENDIX E—Continued

Symbol	Description	Value	Units
F_{xw}	Liquid water mass fraction on precipitation ice species x		
F_{wm}	Maximum mass fraction of liquid water on wet precipitation ice species x	.5	
FN_{xs}	Fractional collection of snow number concentration by wet ice species x		
FQ_{gs}	Fractional collection of snow mass by wet graupel		
FQ_{hs}	Fractional collection of snow mass by wet frozen drops		
FQ_{xs}	Fractional collection of snow mass by wet ice species x		
HM_T	Temperature-dependent factor for Hallett–Mossop rime splintering		
HM_w	Dependence of cloud droplet spectra upon rime splintering		
HM_x	Rimer fall speed dependence upon rime splintering		
HM_{x1}	First factor used to calculate HMV_x		
HM_{x2}	Second factor used to calculate HMV_x		
HMV_x	Rimer fall speed effects upon rime splintering integrated over particle spectra (species x)		$cm^{3+\alpha_x+b_x}$
K_a	Thermal conductivity of air		$J\ m^{-1}\ s^{-1}\ K^{-1}$
$\|K\|_i^2$	Dielectric factor for pure ice	.208	
$\|K\|_w^2$	Dielectric factor for water	.93	
$\|K\|_x^2$	Dielectric factor for ice species x		
L_f	Latent heat of fusion	3.336×10^5	$J\ kg^{-1}$
L_s	Latent heat of sublimation	2.833×10^6	$J\ kg^{-1}$
L_v	Latent heat of vaporization	2.5×10^6	$J\ kg^{-1}$
m_{i0}	Initial mass of a nucleated ice crystal	6.88×10^{-10}	g
m_r	Mass of raindrop of diameter D_r		g
m_s	Mass of snow of diameter D_s		g
m_x	Mass of species x particle of diameter D_x		g
n_g	Graupel number concentration		cm^{-3}
n_h	Frozen drop/hail number concentration		cm^{-3}
n_i	Ice crystal number concentration		cm^{-3}
n_{imax}	Max ice crystal number concentration for ice enhancement		cm^{-3}
n_{in}	Number concentration of nucleated ice crystals		cm^{-3}
n_{in1}	Number concentration of nucleated ice crystals at $T_c \geqslant -5°C$		cm^{-3}
n_{in2}	Number concentration of nucleated ice crystals at $T_c < -5°C$		cm^{-3}
n_{io1}	Constant in ice crystal nucleation at $T_c \geqslant -5°C$		cm^{-3}
n_{io2}	Constant in ice crystal nucleation at $T_c < -5°C$		cm^{-3}
n_{og}	Intercept of graupel size distribution		$cm^{-(4+\alpha_g)}$
n_{oh}	Intercept of frozen drop/hail size distribution		$cm^{-(4+\alpha_h)}$
n_{oi}	Intercept of ice crystal size distribution		$cm^{-(4+\alpha_i)}$
n_{or}	Intercept of rain size distribution		$cm^{-(4+\alpha_r)}$
n_{os}	Intercept of snow size distribution		$cm^{-(4+\alpha_s)}$
n_{ox}	Intercept of size distribution for species x		$cm^{-(4+\alpha_x)}$
n_{oxm}	Intercept for melted ice distribution for species x		$cm^{-(4+\alpha_x)}$
n_{oz}	Intercept of size distribution for species z		$cm^{-(4+\alpha_z)}$
n_{ri}	Number of ice crystals collected by drop of diameter D_r		cm^{-3}
n_{rx}	Number concentration of a redistributed raindrop spectrum		cm^{-3}
n_s	Snow number concentration		cm^{-3}
n_w	Cloud droplet number concentration		cm^{-3}
n_{wl}	Number concentration of large droplets ($\geqslant$25 μm)		cm^{-3}
n_{wl}^*	Number concentration of large droplets rimed onto ice		cm^{-3}
n_{ws}	Number concentration of small droplets ($\leqslant$12 μm)		cm^{-3}
n_{ws}^*	Number concentration of small droplets rimed onto ice		cm^{-3}
n_x	Number concentration of species x		cm^{-3}

APPENDIX E—Continued

Symbol	Description	Value	Units
ΔT_{mlt}	Air temperature after calculating latent heating at $T_c \geqslant 0°C$; prevent unrealistic melting rates		K
ΔV_n	Scaled fall speed difference in number concentration collection kernel, function only of λ_x and λ_z		cm s^{-1}
ΔV_q	Scaled fall speed difference in mass collection kernel, function only of λ_x and λ_z		cm s^{-1}
ϕ	Dispersion of drop distribution		
γ	Air resistance effects on particle fall speed, $(\rho_0/\rho)^{0.5}$		
$\gamma^*(x, y)$	Incomplete gamma function		
Γ	Gamma function		
κ	Exponent in Exner function	.286	
λ_g	Slope of graupel size distribution		cm^{-1}
λ_h	Slope of frozen drop/hail size distribution		cm^{-1}
λ_i	Slope of ice crystal size distribution		cm^{-1}
λ_{i0}	Minimum slope of ice crystals, converted to snow	50	cm^{-1}
λ_r	Slope of rain size distribution		cm^{-1}
λ_s	Slope of snow size distribution		cm^{-1}
λ_{s0}	Minimum slope of snow size distribution	10	cm^{-1}
λ_x	Slope of size distribution for species x		cm^{-1}
λ_{xi}	Slope of size distribution for dry ice species x		cm^{-1}
λ_{xm}	Slope of melted ice distribution for species x		cm^{-1}
λ_z	Slope of size distribution for species z		cm^{-1}
Λ_n	Scale parameter in number concentration collection kernel		$cm^{-(4+\alpha_x+\alpha_z)}$
Λ_q	Scaled parameter in mass collection kernel		$cm^{-(7+\alpha_x+\alpha_z)}$
ν	Kinematic viscosity		cm^2 s^{-1}
Π	Exner function, $(p_0/p)^\kappa$		
θ	Potential temperature		K
ρ	Air density		g cm^{-3}
ρ_g	Density of graupel		g cm^{-3}
ρ_{gi}	Density of dry graupel	.4	g cm^{-3}
ρ_h	Density of frozen drops/hail		g cm^{-3}
ρ_{hi}	Density of dry frozen drops/hail	.9	g cm^{-3}
ρ_L	Density of liquid water	1	g cm^{-3}
ρ_0	Surface air density		g cm^{-3}
ρ_s	Density of snow		g cm^{-3}
ρ_{si}	Density of dry snow	.1	g cm^{-3}
ρ_x	Density of (wet or dry) ice species x		g cm^{-3}
ρ_{xi}	Density of a dry ice species x		g cm^{-3}
ρ_y	Density of ice drop mixture due to collisions between raindrops and precipitation ice		g cm^{-3}
ρ_z	Density of (wet or dry) ice species z		g cm^{-3}
τ_{xy}	Factor used to calculate D_{2xy}		g^{-1} cm^{4-b_x} s^{-1}
ψ	Diffusivity of water vapor in air		cm^2 s^{-1}
ζ	Constant used to adjust deposition rates		

REFERENCES

Adler, R. F., H.-Y. Yeh, N. Prasad, W.-K. Tao, and J. Simpson, 1991: Microwave rainfall simulations of a tropical convective system with a three-dimensional cloud model. *J. Appl. Meteor.*, **30**, 924–953.

Banta, R., and K. R. Hanson, 1987: Sensitivity studies on the continentality of a numerically simulated cumulonimbus. *J. Climate Appl. Meteor.*, **26**, 275–286.

Barth, M. C., D. A. Hegg, and P. V. Hobbs, 1992: Numerical modeling of cloud and precipitation chemistry associated with two rainbands and some comparisons with observations. *J. Geophys. Res.*, **97**, 5825–5845.

Battan, L. J., 1973: *Radar Observation of the Atmosphere.* University of Chicago, 323 pp.

Beard, K. V., and H. R. Pruppacher, 1971: A wind tunnel investigation of the rate of evaporation of small water drops falling at terminal velocity in air. *J. Atmos. Sci.*, **28**, 1455–1464.

Berry, K. X., 1968: Modification of the warm rain process. *Proc. First National Conf. on Weather Modification,* Albany, Amer. Meteor. Soc., 81–88.

Black, R. A., and J. Hallett, 1986: Observations of the distribution of ice in hurricanes. *J. Atmos. Sci.*, **43**, 802–822.

Böhm, H. P., 1989: A general equation for the terminal fall speed of solid hydrometeors. *J. Atmos. Sci.*, **46**, 2419–2427.

Buser, O., and A. N. Aufdermaur, 1973: The density of rime on cylinders. *Quart. J. Roy. Meteor. Soc.*, **99**, 388–391.

Chen, C.-H., 1983: Numerical simulation of tropical convective cloud clusters with ice parameterization. M.S. thesis, Dept. of Atmospheric Science, University of Illinois, 64 pp.

Churchill, D. D., and R. A. Houze, Jr., 1984: Development and structure of winter monsoon cloud clusters on 10 December 1978. *J. Atmos. Sci.*, **41**, 933–960.

Clark, T. L., 1973: Numerical modeling of the dynamics and microphysics of warm cumulus convection. *J. Atmos. Sci.*, **30**, 857–878.

Cotton, W. R., M. A. Stephens, T. Nehkorn, and G. J. Tripoli, 1982: The Colorado State University three-dimensional cloud/mesoscale model—1982. Part II: An ice phase parameterization. *J. Rech. Atmos.*, **16**, 295–320.

——, G. J. Tripoli, R. M. Rauber, and E. A. Mulvihill, 1986: Numerical simulation of the effects of varying ice crystal nucleation rates and aggregation processes on orographic snowfall. *J. Climate Appl. Meteor.*, **25**, 1658–1680.

DeMaria, M., 1985: Linear response of a stratified tropical atmosphere to convective forcing. *J. Atmos. Sci.*, **42**, 1944–1959.

Farley, R. D., 1987: Numerical modeling of hailstorms and hailstone growth. Part II: The role of low-density riming growth in hail production. *J. Climate Appl. Meteor.*, **26**, 234–254.

——, and H. D. Orville, 1986: Numerical modeling of hailstorms and hailstone growth. Part I: Preliminary model verification and sensitivity tests. *J. Climate Appl. Meteor.*, **25**, 2014–2035.

——, P. A. Price, H. D. Orville, and J. H. Hirsch, 1989: On the numerical simulation of graupel/hail initiation via the riming of snow in bulk water microphysical cloud models. *J. Appl. Meteor.*, **28**, 1128–1131.

Ferrier, B. S., W.-K. Tao, and J. Simpson, 1991: Radar and microphysical characteristics of convective storms simulated from a numerical model using a new microphysical parameterization. *Proc. 25th Int. Conf. on Radar Meteorology*, Paris, France, Amer. Meteor. Soc., 782–785.

Flatau, P. J., G. J. Tripoli, J. Verlinde, and W. R. Cotton, 1989: The CSU-RAMS Cloud Microphysical Module: General theory and code documentation. Atmos. Science Paper 451, 88 pp. [Available from Colorado State University, Dept. of Atmospheric Science, Ft. Collins, CO 80523.]

Gamache, J. F., 1990: Microphysical observations in summer MONEX convective and stratiform clouds. *Mon. Wea. Rev.*, **118**, 1238–1249.

Gordon, G. L., and J. D. Marwitz, 1986: Hydrometeor evolution in rainbands over the California valley. *J. Atmos. Sci.*, **43**, 1087–1100.

Hall, W. D., 1980: A detailed microphysical model within a two-dimensional dynamic framework: Model description and preliminary results. *J. Atmos. Sci.*, **37**, 2486–2507.

——, and H. R. Pruppacher, 1976: The survival of ice particles falling from cirrus clouds in subsaturated air. *J. Atmos. Sci.*, **33**, 1995–2006.

Hallett, J., and S. C. Mossop, 1974: Production of secondary ice particles during the riming process. *Nature*, **249**, 26–28.

——, R. I. Sax, D. Lamb, and A. S. R. Murty, 1978: Aircraft measurements of ice in Florida cumuli. *Quart. J. Roy. Meteor. Soc.*, **104**, 631–651.

Hartmann, D. L., H. H. Hendon, and R. A. Houze, Jr., 1984: Some implications of the mesoscale circulations in tropical cloud clusters for large-scale dynamics and climate. *J. Atmos. Sci.*, **41**, 113–121.

Heymsfield, A. J., 1972: Ice crystal terminal velocities. *J. Atmos. Sci.*, **29**, 1348–1357.

——, 1986: Ice particle evolution in the anvil of a severe thunderstorm during CCOPE. *J. Atmos. Sci.*, **43**, 2463–2478.

——, and R. G. Knollenberg, 1972: Properties of cirrus generating cells. *J. Atmos. Sci.*, **29**, 1358–1366.

——, and S. C. Mossop, 1984: Temperature dependence of secondary ice crystal production during soft hail growth by riming. *Quart. J. Roy. Meteor. Soc.*, **110**, 631–651.

——, and J. C. Pflaum, 1985: A quantitative assessment of the accuracy of techniques for calculating graupel growth. *J. Atmos. Sci.*, **42**, 2264–2274.

Hobbs, P. V., 1990: Ice in clouds. *Proc. Conf. on Cloud Physics*, San Francisco, Amer. Meteor. Soc., 600–606.

——, and A. L. Rangno, 1985: Ice particle concentrations in clouds. *J. Atmos. Sci.*, **42**, 2523–2549.

——, and ——, 1990: Rapid development of high ice particle concentrations in small polar maritime cumuliform clouds. *J. Atmos. Sci.*, **47**, 2710–2722.

Houze, R. A., Jr., and D. D. Churchill, 1987: Mesoscale organization and cloud microphysics in a Bay of Bengal depression. *J. Atmos. Sci.*, **44**, 1845–1867.

——, F. D. Marks, Jr., and J. F. Gamache, 1992: Dual-aircraft investigation of the inner core of Hurricane Norbert. Part II: Mesoscale distribution of ice particles. *J. Atmos. Sci.*, **49**, 943–962.

Jorgensen, D. P., and M. A. LeMone, 1989: Vertical velocity characteristics of oceanic convection. *J. Atmos. Sci.*, **46**, 621–640.

Kajikawa, M., and A. J. Heymsfield, 1989: Aggregation of ice crystals in cirrus. *J. Atmos. Sci.*, **46**, 3108–3121.

Koenig, L. R., and F. W. Murray, 1976: Ice-bearing cumulus cloud evolution: Numerical simulation and general comparison against observations. *J. Atmos. Sci.*, **15**, 747–762.

Kogan, Y. L., 1991: The simulation of a convective cloud in a 3D model with explicit microphysics. Part I: Model description and sensitivity experiments. *J. Atmos. Sci.*, **48**, 1160–1189.

Kopp, F. J., H. D. Orville, R. D. Farley, and J. H. Hirsch, 1983: Numerical simulation of dry ice cloud seeding experiment. *J. Climate Appl. Meteor.*, **22**, 1542–1556.

Lau, K.-M., and L. Peng, 1987: Origin of low-frequency (intra-seasonal) oscillations in the tropical atmosphere. Part I: The basic theory. *J. Atmos. Sci.*, **42**, 950–972.

Lew, J. K., D. E. Kingsmill, and D. C. Montague, 1985: A theoretical study of the collision efficiency of small planar ice crystals colliding with large supercooled water drops. *J. Atmos. Sci.*, **42**, 857–862.

Lin, Y.-L., R. D. Farley, and H. D. Orville, 1983: Bulk parameterization of the snow field in a cloud model. *J. Climate Appl. Meteor.*, **22**, 1065–1092.

Lo, K. K., and R. E. Passarelli, Jr., 1982: The growth of snow in winter storms: An airborne observational study. *J. Atmos. Sci.*, **39**, 697–706.

Locatelli, J. D., and P. V. Hobbs, 1974: Fall speeds and masses of solid precipitation particles. *J. Geophys. Res.*, **79**, 2185–2197.

Lord, S. J., H. E. Willoughby, and J. M. Piotrowicz, 1984: Role of a parameterized ice-phase microphysics in an axisymmetric nonhydrostatic tropical cyclone model. *J. Atmos. Sci.*, **41**, 2836–2848.

McCumber, M., W.-K. Tao, J. Simpson, R. Penc, and S.-T. Soong, 1991: Comparison of ice-phase microphysical parameterization schemes using numerical simulations of tropical convection. *J. Appl. Meteor.*, **30**, 985–1004.

Macklin, W. C., 1962: The density and structure of ice formed by accretion. *Quart. J. Roy. Meteor. Soc.*, **92**, 297–300.

Manton, M. J., and W. R. Cotton, 1977: Formulation of approximate equations for modeling moist deep convection on the mesoscale. Atmos. Sci. Paper No. 266, 62 pp. [Available from Colorado State University, Dept. of Atmospheric Science, Ft. Collins, CO 80523.]

Marshall, J. S., and W. M. Palmer, 1948: The distribution of raindrops with size. *J. Meteor.*, **5**, 165–166.

Matson, R. J., and A. W. Huggins, 1980: The direct measurement of the sizes, shapes and kinematics of falling hailstones. *J. Atmos. Sci.*, **37**, 1107–1125.

Meyers, M. P., P. J. DeMott, and W. R. Cotton, 1992: New primary ice-nucleation parameterizations in an explicit cloud model. *J. Appl. Meteor.*, **31**, 708–721.

Mitchell, D. L., 1988: Evolution of snow-size spectra in cyclonic storms. Part I: Snow Growth by vapor deposition and aggregation. *J. Atmos. Sci.*, **45**, 3431–3451.

Mossop, S. C., 1976: Production of secondary ice particles during the growth of graupel by riming. *Quart. J. Roy. Meteor. Soc.*, **102**, 45–57.

——, 1985: Secondary ice particle production during rime growth: the effect of drop size distribution and rimer velocity. *Quart. J. Roy. Meteor. Soc.*, **111**, 1113–1124.

Mugnai, A. H., J. J. Cooper, E. A. Smith, and G. J. Tripoli, 1990: Simulation of microwave brightness temperatures of an evolving hailstorm at SSM/I frequencies. *Bull. Amer. Meteor. Soc.*, **71**, 2–13.

Murakami, M., 1990: Numerical modeling of dynamical and microphysical evolution of an isolated convective cloud—the 19 July 1981 CCOPE cloud. *J. Meteor. Soc. Japan*, **68**, 107–128.

Musil, D. J., 1970: Computer modeling of hailstone growth in feeder clouds. *J. Atmos. Sci.*, **27**, 474–482.

Orville, H. D., and F. J. Kopp, 1977: Numerical simulation of the life history of a hailstorm. *J. Atmos. Sci.*, **34**, 1596–1618.

Passarelli, R. E., Jr., 1978: An approximate analytical model of the vapor deposition and aggregation growth of snowflakes. *J. Atmos. Sci.*, **35**, 118–124.

Pflaum, J. C., and H. R. Pruppacher, 1979: A wind tunnel investigation of the growth of graupel initiated from frozen drops. *J. Atmos. Sci.*, **36**, 680–689.

Potter, B. E., 1991: Improvements to a commonly used cloud microphysical bulk parameterization. *J. Appl. Meteor.*, **30**, 1040–1042.

Pruppacher, H. R., and J. D. Klett, 1978: *Microphysics of Clouds and Precipitation.* Reidel, 714 pp.

Rangno, A. L., and P. V. Hobbs, 1991: Ice particle concentrations and precipitation development in small polar maritime cumuliform clouds. *Quart. J. Roy. Meteor. Soc.*, **117**, 207–241.

Rasmussen, R. M., and A. J. Heymsfield, 1985: A generalized form for impact velocities used to determine graupel accretion densities. *J. Atmos. Sci.*, **42**, 2275–2279.

Rutledge, S. A., and P. V. Hobbs, 1984: The mesoscale and microscale structure and organization of clouds and precipitation in midlatitude cyclones. Part XII: A diagnostic modeling study of precipitation development in narrow cold-frontal rainbands. *J. Atmos. Sci.*, **41**, 2949–2972.

Simpson, J., R. F. Adler, and G. R. North, 1988: A proposed tropical rainfall measuring mission (TRMM) satellite. *Bull. Amer. Meteor. Soc.*, **69**, 278–295.

Smith, E. A., A. Mugnai, H. J. Cooper, G. J. Tripoli, and X. Xiang, 1992: Foundations for statistical–physical precipitation retrieval from passive microwave satellite measurements. Part I: Brightness-temperature properties of a time-dependent cloud-radiation model. *J. Appl. Meteor.*, **31**, 506–531.

Smith, P. L., Jr., 1984: Equivalent radar reflectivity factors for snow and ice particles. *J. Climate Appl. Meteor.*, **23**, 1258–1260.

——, C. G. Myers, and H. D. Orville, 1975: Radar reflectivity factor calculations in numerical cloud models using bulk parameterization of precipitation. *J. Appl. Meteor.*, **14**, 1156–1165.

Soong, S.-T., 1974: Numerical simulation of warm rain development in an axisymmetric cloud model. *J. Atmos. Sci.*, **31**, 1262–1285.

——, and Y. Ogura, 1973: A comparison between axisymmetric and slab-symmetric cumulus cloud models. *J. Atmos. Sci.*, **30**, 879–893.

Srivastava, R. C., 1967: A study of the effects of precipitation on cumulus dynamics. *J. Atmos. Sci.*, **24**, 36–45.

——, 1978: Parameterization of raindrop size distributions. *J. Atmos. Sci.*, **35**, 108–117.

Starr, D. O'C., and S. K. Cox, 1985: Cirrus clouds. Part I: A cirrus cloud model. *J. Atmos. Sci.*, **42**, 2663–2681.

Stewart, R. E., J. D. Marwitz, J. C. Pace, and R. E. Carbone, 1984: Characteristics through the melting layer of stratiform clouds. *J. Atmos. Sci.*, **41**, 3227–3237.

Szoke, E. J., and E. J. Zipser, 1986: A radar study of convective cells in mesoscale systems in GATE. Part II: Life cycles of convective cells. *J. Atmos. Sci.*, **43**, 199–218.

——, ——, and D. P. Jorgensen, 1986: A radar study of convective cells in mesoscale systems in GATE. Part I: Vertical profile statistics and comparison with hurricanes. *J. Atmos. Sci.*, **43**, 182–197.

Takahashi, T., 1976: Hail in an axisymmetric cloud model. *J. Atmos. Sci.*, **33**, 1579–1601.

Tao, W.-K., and S.-T. Soong, 1986: A study of the response of deep tropical clouds to mesoscale processes: Three-dimensional numerical experiments. *J. Atmos. Sci.*, **43**, 2653–2676.

——, and J. Simpson, 1989: Modeling study of a tropical squall-type convective line. *J. Atmos. Sci.*, **46**, 177–202.

——, ——, and M. McCumber, 1989: An ice-water saturation adjustment. *Mon. Wea. Rev.*, **117**, 231–235.

——, ——, S. Lang, M. McCumber, R. Adler, and R. Penc, 1990: An algorithm to estimate the heating budget from vertical hydrometeor profiles. *J. Appl. Meteor.*, **29**, 1232–1244.

——, ——, and S.-T. Soong, 1991: Numerical simulation of a subtropical squall line over Taiwan Strait. *Mon. Wea. Rev.*, **119**, 2699–2723.

——, ——, C.-H. Sui, B. Ferrier, S. Lang, J. Scala, M.-D. Chou, and K. Pickering, 1993: Heating, moisture and water budgets of tropical and midlatitude squall lines: Comparisons and sensitivity to longwave radiation. *J. Atmos. Sci.*, **50**, 673–690.

Trenberth, K. E., G. W. Branstator, and P. A. Arkin, 1988: Origins of the 1988 North American drought. *Science*, **242**, 1640–1645.

Uplinger, W. G., 1981: A new formula for raindrop terminal velocity. *Proc. 20th Conf. on Radar Meteorology*, Boston, Amer. Meteor. Soc., 389–391.

Verlinde, J., P. J. Flatau, and W. R. Cotton, 1990: Analytical solutions to the collection growth equation: Comparison with approximate methods and application to cloud microphysics parameterization schemes. *J. Atmos. Sci.*, **47**, 2871–2880.

Williams, R., and P. J. Wojtowicz, 1982: A simple model for droplet size distribution in atmospheric clouds. *J. Appl. Meteor.*, **21**, 1042–1044.

Willis, P. T., 1984: Functional fits to some observed drop size distributions and parameterization of rain. *J. Atmos. Sci.*, **41**, 1648–1661.

——, and A. J. Heymsfield, 1989: Structure of the melting layer in mesoscale convective system stratiform precipitation. *J. Atmos. Sci.*, **46**, 2008–2025.

——, and J. Hallett, 1991: Microphysical measurements from an aircraft ascending with a growing isolated maritime cumulus tower. *J. Atmos. Sci.*, **48**, 283–300.

Wisner, C., H. D. Orville, and C. Myers, 1972: A numerical model of a hail-bearing cloud. *J. Atmos. Sci.*, **29**, 1160–1181.

Yeh, H.-M., N. Prasad, R. A. Mack, and R. F. Adler, 1990: Aircraft microwave observations and simulations of deep convection from 18 to 183 GHz. Part II: Model results. *J. Atmos. Oceanic Technol.*, **7**, 392–410.

Young, K. C., 1975: The evolution of drop spectra due to condensation, coalescence and breakup. *J. Atmos. Sci.*, **32**, 965–973.

Ziegler, C. L., 1985: Retrieval of thermal and microphysical variables in observed convective storms. Part I: Model development and preliminary testing. *J. Atmos. Sci.*, **42**, 1487–1509.

——, 1988: Retrieval of thermal and microphysical variables in observed convective storms. Part II: Sensitivity of cloud processes to variation of the microphysical parameterization. *J. Atmos. Sci.*, **45**, 1072–1090.

Zipser, E. J., and M. A. LeMone, 1980: Cumulonimbus vertical velocity events in GATE. Part II: Synthesis and model core structure. *J. Atmos. Sci.*, **37**, 2458–2469.